

Scale-Invariant Strength Assortativity of Streaming Butterflies

AIDA SHESHBLOUKI, University of Waterloo, Canada

M. TAMER ÖZSU, University of Waterloo, Canada

Bipartite graphs are rich data structures with prevalent applications and identifier structural features. However, less is known about their growth patterns, particularly in streaming settings. Current works study the patterns of static or aggregated temporal graphs optimized for certain down-stream analytics or ignoring multipartite /non-stationary data distributions, emergence patterns of subgraphs, and streaming paradigms. To address these, we perform statistical network analysis over web log streams and identify the governing patterns underlying the bursty emergence of mesoscopic building blocks, 2,2-bicliques known as butterflies, leading to a phenomenon that we call “scale-invariant strength assortativity of streaming butterfly”. We provide the graph-theoretic explanation of this phenomenon. We further introduce a set of micro-mechanics in the body of a streaming growth algorithm, *sGrow*, to pinpoint the generative origins. *sGrow* supports streaming paradigms, emergence of 4-vertex graphlets, and provides user-specified configurations for the scale, burstiness, level of strength assortativity, probability of out-of-order records, generation time, and time-sensitive connections. Comprehensive Evaluations on pattern reproducing and stress testing validate the effectiveness, efficiency, and robustness of *sGrow* in realization of the observed patterns independent of initial conditions, scale, temporal characteristics, and model configurations. Theoretical and experimental analysis verify the *robust* ability of *sGrow* in generating streaming graphs based on user-specified configurations that affect the scale and burstiness of the stream, level of strength assortativity, probability of-of-order streaming records, generation time, and time-sensitive connections.

CONTENTS

Abstract	1
Contents	2
1 Introduction	3
2 Preliminaries and datasets	6
3 Assortativity Analysis in Graph Streams	8
3.1 The Proposed Strength Assortativity Quantification Approach	10
4 Butterfly Emergence Patterns	11
4.1 Analysis of Real-world Graph Streams	11
4.2 Related Works on Modeling of Graph Patterns - A Brief Survey	14
4.3 Analysis of Microscopic Growth Mechanisms	16
4.4 Discussion	17
5 The proposed Streaming Growth Model: sGrow	21
5.1 Overview	22
5.2 Data Structures	23
5.3 Strength Preferential Selection	24
5.4 Preferential Random Walk	25
5.5 Burst Addition	26
6 Evaluations	26
6.1 Computational Complexity	27
6.2 Pattern Reproducing	29
6.3 Stress testing	30
6.3.1 Effectiveness	33
6.3.2 Efficiency	33
6.3.3 Burst Size	33
6.3.4 Parameter Configuration	33
6.4 Discussion	34
7 Conclusion	36
References	37

1 INTRODUCTION

We study the bursty emergence of meso-scale building blocks in bipartite streaming graphs representing web logs to uncover the crucial mixing patterns and identify/explain their microscopic generative origins by introducing a streaming growth model. All complex networks have an underlying bipartite structure [46, 109]. Even those networks that are naturally unipartite, e.g. social networks, have an inherent bipartite structure driving the topological structure of the unipartite version [46, 85, 108, 109]. These bipartite structures are captured by bipartite graphs, which are rich data models that provide full representation without information loss for interactions that naturally occur in one mode (compressed datasets as unipartite graphs [128]), or multiple modes (high order interconnections as hyper graphs [5, 57, 114]). A prevalent use case is where bipartite graphs capture the interactions of users with entities spanning different domains such as social networks (users-hashtags [122]), web-based services (users-websites, multimedia services, and products [58, 102, 105, 112, 117]), financial systems (users-donation campaigns [4]), transportation systems (users-registered vehicles [59]), and communication systems (users-phone calls [120]).

Despite the widespread applications, richness and critical role in determining the topological properties, less is known about the growth and generative patterns of bipartite interconnected data particularly in streaming settings [22] where the continuous rapid temporal evolutions lead to unbounded/unknown stream length and non-stationary distributions of the underlying data snapshots. In this context, the temporal evolutions usually occur wrt the most recent graph topology (i.e. update events are not global); the evolving streaming rates leads to non-uniform inter-event statistics; and multiple generative sources (as well as factors such as transmission delays) cause out-of-order arrival of data records to a processing unit which has no control over the arrival order or data rate [42, 89]. Streaming graphs are different from aggregated temporal graphs that are a sequence of graph snapshots (representing a dynamic graph with an entirely available structure that undergoes temporal changes). Moreover, weight addition patterns [80], streaming context [88], and data-driven semantics [9] lead to burstiness in streaming record arrivals. An example is the case of user-product interactions in Alibaba e-commerce services that incurred a processing rate of 470 million event logs per second during a peak interval [88]. Current works study and model the generative patterns of static or aggregated temporal graphs commonly optimized for down stream analytics or ignore (1) multipartite/non-stationary data distributions, (2) *emergence* patterns (not just existence) of building blocks, and (3) streaming paradigms such as unbounded/time-sensitive updates, evolving streaming rates, and out-of-order/bursty records (e.g., [3, 6, 12, 43, 70, 112, 121, 126]). In this paper, we perform statistical analysis over web log streams to infer the key features governing the emergence of the mesoscale building blocks of the bipartite streaming graphs.

Mesoscopic network inference. Frequent subgraphs (motifs [81] or graphlets [97]) as the building blocks of graphs [81] play an important role in understanding the structure of graphs [1, 19, 55, 63, 74, 77, 79, 90, 95, 97–99, 103, 113, 118, 121]. Particularly, the presence of butterflies (2, 2-bicliques) as the simplest and most local form of cycles in the bipartite graphs has been identified as the main driver of transitivity and degree assortativity in the corresponding unipartite graphs (projections) [109]. Moreover, butterflies are of great importance in measuring properties such as cohesion, network stability and error tolerance [129]. Recently, various butterfly-based data models and analytic algorithms have been proposed for measuring rectangle-based connectivity, estimation of maximal bicliques and bitruss decomposition in heterogeneous information networks [6, 31, 36, 51, 73, 124]. In a previous study [98], we have shown that butterflies are temporal motifs with bursty emergence patterns giving rise to significantly higher occurrence numbers over the timeline of edge arrivals compared to random (null) graphs. The quantitative emergence pattern is formulated as the butterfly densification power law (BPL) which states that the number of butterflies at time

t follows a power law function of the number of edges at time t . In real world graphs displaying BPL, there is a strong positive correlation between the butterfly support and degree of vertices and the probability of butterflies incorporating hubs (i.e. vertices with degree higher than average unique degree of seen vertices) is high. Also, there is a correlation between the frequency and average degree of hubs with the frequency of butterflies. Hence, the hubs are identified as the main contributors to bursty formation of butterflies. However, BPL does not happen in random bipartite graphs constructed by the preferential attachment model. In preferential attachment model [8], the degree of hubs increases over time with the arrival of new vertices; however, the number of butterflies does not grow as rapidly as that of real-world graphs. Therefore, there exist other factors besides the vertex degree that are impactful in butterfly densification. In this study, our goal is to discover these factors. We aim to answer two questions: *how do butterflies as the building blocks of bipartite streaming graphs emerge over time?* and *what is the generative process underlying their emergence?* The answers to these questions allow us to model the realistic growth patterns in bipartite streaming graphs. To further focus our research, we investigate the organizing principles in web-based user-item streams. The sequences of user-item interactions in web-services are typically associated with a weight that can be an explicit value such as rating, or an implicit value denoting the multiplicity of interactions between a pair of vertices. Moreover, the time-labeled interactions are continuously generated with a non-stable rate giving rise to emergence of an unbounded dynamic structure. The edge weights and fine grained temporal information enable exploring the temporal and connectivity patterns. We use publicly available data in which the timestamp and weight are explicitly given in the data records (common in rating graphs). We do not consider implicit weights computed by aggregating multiple edges between two vertices since such aggregations require aggregating the timestamps as well, which in turn manipulates the temporal properties and makes the temporal analysis unreliable. We study the bipartite structures directly as opposed to investigating the unipartite projections. Although projection enables using standard tools for analyzing unipartite graphs, three main issues exist: (1) information loss as the projection is not bijective and timestamps and weights are not captured in projection, (2) edge inflation as high degree vertices are transformed to dense cliques, and (3) unreliable patterns such as community structure and degree mixing patterns rooted from artificial edge densification and subgraph formation [15, 44, 46, 48, 68, 86].

Contributions. We explore the preference of vertices forming butterflies to connect to each other wrt strength similarity (i.e. strength assortativity) by integrating the vertex degrees and edge weights as vertex strength and considering burst of edges. To this end, we show the limitation of conventional approaches to study such mixing patterns and introduce a new quantification approach, based on tracking the localization of a vector embedding the data distributions in sequential burst-based graph snapshots, to enable effective temporal analysis of strength assortativity in graphs having abundant cliques, different scales, and multiple/skewed strength distributions; Utilizing this approach, we unveil the “scale-invariant strength assortativity of streaming butterflies” which represents a co-occurrence of three patterns:

- (1) *Butterfly densification*: The butterfly count grows super-linearly wrt the edge count.
- (2) *Strength diversification*: Butterflies display a wide range of vertex strengths with a right skewed distribution and the skew increases over time.
- (3) *Steady strength assortativity*: Butterflies display a stable strength assortativity since the right skewed distribution of strength difference of connected butterfly vertices is fixed-shape, although the skew increases over time, and strength differences are localized below the mean.

The co-occurrence of these patterns is counter-intuitive and interesting: As the stream and the number of butterflies grow rapidly, we observe that diversity of strengths for butterfly vertices

increases and strong (i.e. high strength) vertices get stronger and obtain weak neighbors with the increasing of variance of strength differences. Therefore, we expect an increasing trend of disassortativity. However, the majority of butterfly edges are formed by vertices with similar strength and this assortativity remains at a fixed level regardless of stream size or butterfly count. Therefore, the co-occurrence of these patterns implies non-trivial mixing patterns. Moreover, our analyses of existing growth mechanisms that yield skewed distributions, degree correlation, and cohesive structures highlight the essence of new growth models. We explain the confounding data-driven semantics in the domain of user-item interactions as these patterns relate to three graph theory concepts: burstiness, rich-get-richer, and core-periphery. Furthermore, we introduce *sGrow*, a streaming growth model that explains the observed patterns and preserves related concepts. *sGrow* is based on addition of edge bursts which satisfies streaming data paradigms, preserves realistic patterns quantitatively and qualitatively, and also makes the stream generation scalable. Moreover, *sGrow* enables generating a sequence of bipartite edges attributed with timestamps and weights, isolated/out-of-order edges, and four-vertex graphlets. Our evaluations validate that *sGrow* efficiently and effectively reproduces the bursty emergence patterns of streaming butterflies, independent of initial conditions, scale, temporal characteristics, and model configurations. Our experiments also verify the robustness of *sGrow* in generating realistic streaming graphs configured with user-specified properties that affect generation time, scale and burstiness of the stream, level of strength assortativity, probability of out-of-order streaming records, and time-sensitive connections. Our contributions in this paper are the following:

- A new measure for assortativity analysis. We introduce an effective quantification approach for mesoscale mixing patterns in weighted bipartite streaming graphs which is also applicable to static and/or unipartite graphs.
- Butterfly emergence patterns. We uncover the *scale-invariant strength assortativity of streaming butterflies* rooted from three real-world streaming graph patterns (butterfly densification, strength diversification, and steady strength assortativity) and three graph theory concepts (burstiness, rich-get-richer, and core-periphery).
- A streaming growth model. We introduce *sGrow*, a streaming growth algorithm that explains the observed patterns and preserves the confounding concepts while supporting streaming paradigms, emergence of 4-vertex graphlets, and user-specified configurations. Accordingly, we introduce:
 - A reference guide supported by extensive stress-testing experiments for configuring the parameters in benchmarking applications.
 - A set of microscopic mechanisms to benefit development of streaming algorithms and optimized-models.

Impact. While our quantification approach can benefit network inference over temporal graphs, our analysis of bipartite graph streams and our growth model are impactful in the following cases:

- *Streaming graph benchmarks.* Performance evaluation of algorithms including but not limited to butterfly-based algorithms relies on considering the characteristics of input graphs [11, 12, 21]. Given the lack of streaming graph generators, our work help understand the important graph characteristics as well as providing realistic *configurable* and scalable graphs for stress testing purposes.
- *Machine learning benchmarks.* Collecting/annotating the training/testing datasets for graph-based models in domains such as outlier detection and computer vision is challenging due to the nature of data (e.g., rare outliers and diverse image instances), and expenses of manually labeling the instances [91, 112, 123]. Solutions include building benchmark datasets via artificial instance injection [23, 35, 123] and applying weakly-supervised techniques [45,

78, 112]. Our analytical approach can be extended to such domains to inform the design of graph-based models with the temporal connectivity patterns and also generating realistic yet synthetic datasets to which the artificial instances are injected.

- *Concept drift modeling.* To improve the performance of online adaptive learning algorithms in stream-based recommender systems for web activities, it is important to consider the temporal evolution of modeled concepts due to a change in the distribution of log data or a change in the relation between data and target variable (i.e. concept drift) [7, 40, 96]. Considering a butterfly as two users with mutual preferences and two items with mutual perceptions, our work impacts modeling the parallel drift of concepts such as user preferences and item perception.
- *Algorithm developments.* Graph analytics and generative models utilize microscopic mechanisms and graph pattern for algorithm design [98, 112]. Our microscopic mechanisms and growth patterns benefit these cases as well.

The rest of paper is organized as following: Section 2 reviews preliminaries and datasets; Section 3 introduces a new perspective for strength assortativity quantification; Section 4 is devoted to our observations in real-world and synthetic streams as well as a brief survey of related works on graph patterns and growth rules; Section 5 introduces sGrow; Section 6 reports the evaluations; Section 7 concludes the paper.

2 PRELIMINARIES AND DATASETS

We denote a bipartite graph as $G = (V, E)$, where $V = V_i \cup V_j$, $V_i \cap V_j = \emptyset$ and $E \subseteq V_i \times V_j$. We refer to $V_i = \{v_i\}$ and $V_j = \{v_j\}$ as i-vertices and j-vertices. We denote the set of immediate/nearest neighbors of an i-vertex v_i , called j-neighbors, as $N_j(v_i)$; similarly for i-neighbors $N_i(v_j)$.

Definition 2.1 (Streaming Graph Record). A streaming graph record (sgr) is a quadruple $r^m = \langle v_i^m, v_j^m, \omega_{ij}^m, \tau^m \rangle$ where m is the sgr index, ω_{ij}^m is the weight of the edge between v_i and v_j , and τ^m is the timestamp of the sgr assigned by the generative source.

Definition 2.2 (Weighted Bipartite Streaming Graph). A weighted bipartite streaming graph is an unbounded sequence of sgrs denoted as $\mathfrak{R} = \langle r^1, r^2, \dots \rangle$.

The sequence of sgrs can be ordered by either timestamps or arrival times. We consider the latter to support out-of-order sgrs (late arrivals).

Definition 2.3 (Burst). A burst is the batch of subsequent sgrs with same timestamp. The number of bursts in the stream is denoted as N_b and equals to the number of unique timestamps.

We highlight that a burst is the batch of *subsequent*, not *all*, sgrs with same timestamp. This definition enables burst-based analysis of out-of-order sgrs.

Definition 2.4 (Burst-based Graph Snapshot). A burst-based graph snapshot, G_{N_b} , is the bipartite graph formed by the prefix of sgrs seen since the first timestamp τ^1 until N_b -th unique timestamp. i.e. $G_{N_b} = (V, E)$, s.t. $V = V_i \cup V_j$, $V_i \cap V_j = \emptyset$, $E \subseteq V_i \times V_j$, and $E = \{r^m | \tau^m \in [\tau^0, \tau^{N_b}]\}$.

Weighted bipartite streaming graphs display bursty patterns since (1) weight additions in temporal graphs follow bursty patterns [80], (2) data streams are commonly characterized as bursty [89, 125], and (3) data-driven semantics imply burstiness (for instance, human-initiated events are driven by the queuing processes of human decision making leading to non-Poisson inter-event statistics [9]). That is why real-world user-item interactions are characterized as bursty and the distribution of timestamps change over time. In other words, groups of interactions occur in short periods of intense activity (bursts) separated by relatively long gaps of inactivity. We study user-item data

sets and due to the bursty characterization of these data streams, we conduct our analysis over graph snapshots created based on the number of bursts in the stream. This enables comparing the graph snapshots at different scales (number of vertices/edges) and also evaluating the temporal properties in parallel to structural analyses.

Definition 2.5 (Vertex Strength). Vertex strength (shortly strength) is defined as the total weight of edges connected to the vertex, $S_i = \sum_{j \in N_j(i)} \omega_{ij}$, $S_j = \sum_{i \in N_i(j)} \omega_{ij}$ [16, 17, 100].

Vertex strength is a natural generalization of the connectivity of graphs and is considered as a significant measure of graph properties in terms of weights [17]. We use this notion for parallel study of edge weights and vertex degrees and their impact on the emergence patterns of butterflies.

Datasets– We use seven real-world graph datasets: Ciao [49], Epinions [104], WikiLens [39], MovieLens100k (ML100k) [53], MovieLens1m (ML1m) [52], Amazon [61, 75, 83], and Yahoo songs (Yahoo) [34]. All datasets are available at public repositories KONECT [67] and Netzscheuler [94]. These datasets include naturally occurring bipartite interactions as a set of records including the user ID, item ID, rating, and timestamp. The rating values are in the set $\{1, 2, 3, 4, 5\}$ in all datasets except for WikiLens with ratings in $\{0, 0.5, 1, \dots, 4.5, 5\}$. In WikiLens, we rounded the ratings and replaced ratings equal to 0 with 1 to convert the rating scale to $1 - 5$. Table 1 provides the statistics of all the graph streams. These streams cover different structural properties (edge density, average vertex degree, and wedge (i.e. two-path) count) and temporal characteristics (number and average size of bursts). Ciao and Amazon have low average degree of both i - and j -vertices, while they are bursty streams. Epinions has higher average degree of i -vertices compared to that of j -vertices with a very high number of wedges (the building blocks of butterflies), and it is a bursty stream with large bursts. WikiLens has high average degree of i -vertices but it is not bursty. ML100k has high average degree of i - and j -vertices and high number of wedges and it is roughly as bursty as ML1m and Yahoo which have higher average degree of i - and j -vertices and higher number of wedges.

Table 1. Real-world user-item graph datasets. d_i and d_j denote the average degree of i -vertices and j -vertices, respectively. N_b and $b = |E|/N_b$ denote the number and the average size of bursts, respectively. \wedge denotes the number of wedges (two-paths).

	$ V_i $	$ V_j $	$ E $	d_i	d_j	N_b	b	\wedge
Ciao	17, 615	16, 121	72, 665	4.1	4.5	4, 919	14.8	4, 896, 641
Epinions	120, 492	755, 760	13, 668, 320	113.4	18	501	27, 282	69, 245, 866, 714
WikiLens	326	5, 111	26, 937	82.6	5.2	26, 239	1	6, 316, 744
ML100k	943	1, 682	100, 000	106	59.4	49, 282	2	18, 367, 254
ML1m	6, 040	3, 706	1, 000, 210	165.6	269.9	458, 455	2.2	602, 009, 923
Amazon	2, 146, 057	1, 230, 915	5, 838, 041	2.7	4.7	3, 329	1, 753.7	627, 186, 651
Yahoo	1, 000, 990	624, 961	256, 804, 235	256.5	410.9	105, 331, 405	2.4	4, 627, 224, 528, 654

Our analyses rely on exact butterfly listing over landmark windows which is computationally expensive in bursty streams. We use the exact algorithm in sGrapp suit [98] to list the butterflies over sequential **burst-based graph snapshots**. We study the emergence of a certain number of butterflies in different streams with different structural/temporal properties. That is, we consider the prefix of streams until the arrival of up to $\approx 6.5 \times 10^6$ butterflies which covers the entire stream in WikiLens with 26220 bursts and a prefix of 10000, 9600, 460, 2000, and 15000 bursts in ML1m, ML100k, Epinions, Amazon, and Yahoo, respectively. In Ciao, we checked the entire stream with 4900 bursts and $\approx 6.4 \times 10^5$ butterflies (Table 2). We divide the corresponding timeline of burst arrival into 20 equally distanced points and at each point we study the butterflies in the burst-based graph snapshot (Definition 2.4). In our analyses we care about the value and the trend of data points

and the number of graph snapshots (here 20) just change the smoothness of the plots and does not affect the results since we check streams with different distribution of timestamps and the scale of graph snapshots differs in various streams. The number of edges/butterflies in each burst varies in different graphs depending on the burstiness of the graph stream.

Table 2. The number of edges $|E^{20}|$, the number of bursts N_b^{20} , and the butterfly count \bowtie^{20} of the 20th graph snapshot in real-world graph streams.

	$ E^{20} $	N_b^{20}	\bowtie^{20}
Ciao	72,574	4,900	636,440
Epinions	296,665	460	6,418,862
WikiLens	26,918	26,220	6,556,913
ML100k	18,696	9,600	6,492,834
ML1m	22,795	10,000	6,678,784
Amazon	2,194,798	2,000	6,496,236
Yahoo	42,105	15,000	6,496,563

3 ASSORTATIVITY ANALYSIS IN GRAPH STREAMS

The tendency of vertices to connect to similar vertices with respect to one of their quantitative/qualitative attributes is called assortativity/homophily [84]. In addition to connectivity insights (our primary goal in this paper), assortativity provides information about the dynamic behavior and robustness of the graph [29, 106]. For instance, degree disassortative complex networks compared to degree assortative networks exhibit higher epidemiological threshold leading to easier immunization, however assortative networks get higher resilience to systemic risk by degree-targeted immunization policies [29] (see [87] for a complete survey). Assortativity is usually studied with respect to vertex degrees. A previous study [72] has shown that studying the assortativity by considering just the degree does not completely uncover the organizational patterns in the structure of graphs. Leung and Chau [72] have introduced the weighted assortativity coefficient to measure the tendency of having a high-weighted edge between vertices with similar degrees. However, we are interested in strength assortativity, i.e. measuring the tendency of having an edge between vertices with similar strength, particularly in butterflies. In this section, we first establish the requirements for an effective measurement of strength assortativity that can accommodate analysis of mesoscopic, bipartite, and temporal structures; next, we introduce a new metric for strength mixing patterns called strength assortativity localization factor.

The assortativity coefficient (r) [84] is a common metric for assortativity [107, 109, 130]. Assuming that we are interested in quantifying the tendency of vertices to connect to each other based on the similarity of their attribute K , r is computed as the pearson correlation of K of linked vertices and lies in the range $-1 \leq r \leq 1$. Positive (negative) r signals (dis)assortativity and $r = 0$ denotes random mixing. Another approach to study assortativity is to compute the average K of nearest-neighbors for each vertex and then aggregating the values by restricting the class of vertices with $K = k$. We denote it as $\langle K_n \rangle$ which is a function of K . An increasing (decreasing) $\langle K_n \rangle$ signals (dis)assortativity. This can be inferred by checking the sign of the slope of a linear fit for log-log plot of $\langle K_n \rangle$ as a function of K . In the following, we investigate the effectiveness of r and $\langle K_n \rangle$ in quantifying the strength assortativity of butterflies.

We consider the evolution of two distributions over sequential graph snapshots: (1) $Pr(\delta)$, the probability distribution of strength difference for connected butterfly vertices which is computed as $Pr(\delta) = \frac{F(\delta)}{\sum F(\delta)}$, where $F(\delta)$ is the number of edges with strength difference δ and the sum runs

over the range of δ values, and (2) $Pr(S_i)$, the probability distribution of strength for butterfly i-vertices which is computed as $Pr(S_i) = \frac{F(S_i)}{\sum F(S_i)}$, where $F(S_i)$ is the number of butterfly i-vertices with strength S_i . The same notations stand for j-vertices and $Pr(S_j)$.

As a running example in this section, we use the real-world graph stream Epinions and pick 20 equally-distanced points in the timeline of burst arrival. At each point (N_b), we calculate r for the strengths of linked butterfly vertices in the corresponding graph snapshot G_{N_b} (Figure 1.a). We also consider $Pr(\delta)$ at two points corresponding to the arrival of 92 (Figure 1.d) and 437 bursts (Figure 1.g). At $N_b = 92$, the probability that a butterfly edge has strength difference below the average strength difference μ_δ is $Pr(\delta \leq \mu_\delta) = 0.67$. However, the assortativity coefficient is $r = 0.007$ suggesting no (dis)assortativity (i.e. random connection of butterfly vertices with no tendency to connect to (dis)similar vertices). Also, at $N_b = 437$, we observe that majority of butterfly edges fall in the region behind μ_δ with probability $Pr(\delta \leq \mu_\delta) = 0.71$, while $r = -0.17$ suggests strength disassortativity.

The reason behind this confusing behavior of r is its bias toward the distribution of strength of i- and j-vertices with respect to their average. To clarify, we consider $Pr(S_i)$ and $Pr(S_j)$ at these two time points (Figure 1.e,f,h,i). At $N_b = 92$, the probability that a butterfly i(j)-vertex has strength less than or equal to the average strength of butterfly i(j)-vertices $\mu_i(\mu_j)$ is almost equal to the probability that a butterfly i(j)-vertex has strength greater than the average strength of butterfly i(j)-vertices ($Pr(S_i \leq \mu_i) = 0.57$ and $Pr(S_j \leq \mu_j) = 0.54$). Therefore, many strength deviations from the mean strength, particularly for j-vertices, would be zero, making the coefficient an insignificant value close to zero ($r = 0.007$). At $N_b = 437$, a large majority of butterfly i(j)-vertices have strength above the average strength of butterfly i(j)-vertices ($Pr(S_i > \mu_i) = 0.9$, $Pr(S_j > \mu_j) = 0.8$), therefore their high deviations from the mean lowers the coefficient. In summary, the assortativity coefficient reflects the global correlation between $Pr(S_i)$ and $Pr(S_j)$ (two separate distributions). The assortativity coefficient fails to capture the pairwise correlations between strength of connected i- and j-vertices forming butterflies.

We examine the neighborhood-based approach for studying assortativity. Figures 1.b-c, show the nearest-neighbor average strength of vertices with strength S [93]. At first glance, the decreasing trend suggests strength disassortativity: the higher the strength of a vertex, the lower the average strength of its neighbors and vice versa. However, we should consider the skewed $Pr(S_i)$ and $Pr(S_j)$ with high-strength vertices. Suppose that low-strength vertices are connected to many low-strength vertices and one high-strength vertex. In this case, the average strength of neighbors for these low-strength vertices would be high although the majority of neighbors have similar low strengths. That is, relatively few vertices having high strengths (because of many connections and/or connections with high weights) skew the average strength of their low-strength neighbors and hence mislead the assortativity interpretation. This again highlights the issue of measuring strength assortativity in graphs with broad and skewed strength distribution.

To conclude, using conventional assortativity metrics is not reliable for analyzing the strength assortativity of butterflies in bipartite streaming graphs since (1) r is vertex-centric and reflects the global strength correlations rather than pairwise strength correlations. Particularly, in case of butterflies that each vertex contributes duplicate values because of two adjacent edges, vertices with strength equal/close to the mean (zero $S - \mu$), decrease the overall correlation, no matter what the strength of their neighbor is, (2) r is designed for unipartite graphs and using it in bipartite graphs can bias the outcome by the strength distributions of i- and j-vertices, and (3) The neighborhood-based approach can be misleading in case of graphs with broad and skewed strength distributions since high-strength vertices have outlier impacts and make the interpretation difficult.

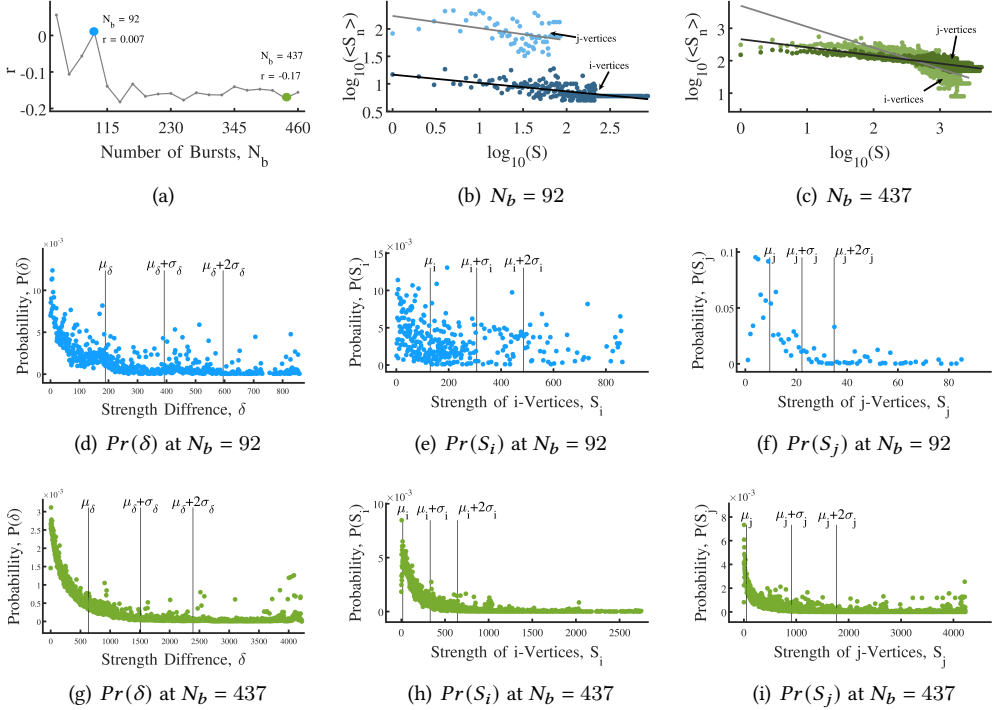


Fig. 1. (a) Assortativity coefficient over timeline of burst arrival in Epinions stream. Nearest-neighbor average strength of vertices with strength S at (b) $N_b = 92$ and (c) $N_b = 437$. Distribution of strength differences of connected butterfly vertices at (d) $N_b = 92$ and (g) $N_b = 437$. Distribution of strength of butterfly (e,h) i-vertices and (f,i) j-vertices at $N_b = 92$ and $N_b = 437$, respectively.

3.1 The Proposed Strength Assortativity Quantification Approach

Informed by the above discussion, an appropriate measure for the tendency of vertices to connect to vertices with similar strength that is applicable to butterfly edges should satisfy the following properties: (1) it should directly reflect the probability distribution of strength differences rather than the global correlations in the distribution of strengths; (2) it should not be designed based on neighbor information since in case of skewed distribution of strengths, it would be biased by the outlier vertices; and (3) it should enable comparison of strength assortativity for sequential graph snapshots in the same stream as well as comparison of strength assortativity of graph snapshots in different graph streams.

Our goal is to quantify and compare the distribution of strength differences in low dimension to enable temporal analysis over sequential graph snapshots of streams. A common approach for comparing distributions (usually degree distributions) is Kolmogorov-Smirnov test. However, this is sensitive to the distribution range and is not ideal for analyzing sequential graph snapshots and different graph streams. The Degree Distribution Quantification and Comparison (DDQC) approach [10] quantifies the degree distribution of a graph based on $4 \times 2^\beta$ regions in the degree distribution and uses this quantification for comparison. The regions are determined in two steps: first, the degree distribution is divided into four regions covering the intervals between five

subsequent points: $\min(\text{degree})$, $\mu - \alpha\sigma$, μ , $\mu + \alpha\sigma$, and $\max(\text{degree})$, where μ is the mean degree and σ is the standard deviation of degrees and α is a configurable parameter. Next, each region is divided into 2^β equal sub-regions, where β is the second configurable parameter. Given these regions in the probability distribution, a vector is constructed with $4 \times 2^\beta$ elements each representing the summation of probabilities in a corresponding region.

We consider the probability distribution of strength difference of connected butterfly vertices $Pr(\delta)$ given a graph snapshot G_{N_b} . Using burst-based snapshots enables fair comparison of different graphs with different temporal characteristics. Inspired by the DDQC approach, we divide $Pr(\delta)$ into four regions based on the mean and standard deviation of δ s (μ_δ and σ_δ , see Figure 1.d,g). As long as the first region covers the low δ s, the number/coverage of other regions for the tail of right-skewed distribution is not impactful in mixing pattern analysis. Accordingly, we summarize the probability distribution as an embedding vector F with four elements ($\sum_{i=1,\dots,4} F_i = 1$). Each element corresponds to a region as below:

$$F_1 = \sum Pr(\delta), \forall \delta \leq \mu_\delta \quad (1)$$

$$F_2 = \sum Pr(\delta), \forall \mu_\delta < \delta \leq \mu_\delta + \sigma_\delta \quad (2)$$

$$F_3 = \sum Pr(\delta), \forall \mu_\delta + \sigma_\delta < \delta \leq \mu_\delta + 2\sigma_\delta \quad (3)$$

$$F_4 = \sum Pr(\delta), \forall \delta > \mu_\delta + 2\sigma_\delta \quad (4)$$

The vector F provides fine-grained information. Additionally, to express the strength assortativity as a scalar for simple network inference in temporal analyses, we define the *strength assortativity localization factor* as $r^s = F_1 - 0.5$ to track the localization of δ s (F) on the region behind mean (F_1). r^s lies in the range $[-0.5, 0.5]$. A (negative) positive r^s highlights strength (dis)assortativity and a zero value corresponds to random strength mixing. $r = 0.5$ denotes perfect strength assortativity and $r = -0.5$ denotes perfect strength disassortativity.

4 BUTTERFLY EMERGENCE PATTERNS

In this section, we analyze the butterfly emergence patterns in streaming graphs. We start by analyzing the real-world streaming graphs to identify the characteristic mixing patterns of butterflies (§ 4.1). We then briefly survey the related works on graph patterns and growth models (§ 4.2). Next, we study synthetic streaming graphs based on seminal structure growth models to explain the generative processes underlying the observed patterns (§ 4.3). Finally, we discuss our findings (§ 4.4).

4.1 Analysis of Real-world Graph Streams

Figure 2 shows the growth of butterfly count in real-world streams. To quantify this growth, we define the butterfly rate of each graph snapshot as the number of butterflies (\bowtie) in the graph normalized by the number of edges ($|E|$), $\bowtie / |E|$, and compute the average butterfly rate (plus/minus the standard deviation) over the sequential snapshots. As provided in Figure 2, the average butterfly rate is greater than 1 in all streams, indicating that the number of butterflies grows superlinearly with respect to the number of edges in the sequential graph snapshots. In some graphs the superlinearity starts after some time.

We compute $Pr(\delta)$, the probability distribution of strength-differences of connected butterfly vertices, for the graph snapshots in the streams. We embed each probability distribution in a vector F as explained in § 3.1. Figures 3 and 4 demonstrate the evolution of F elements and their corresponding strength assortativity localization factor (r^s) over the timeline of burst arrivals. We observe that in all graph streams, butterfly edges have strength-difference less than equal to the average strength-difference (μ_δ) with probability $Pr(\delta \leq \mu_\delta) \approx 0.7$ (F is localized on F_1). The tail of

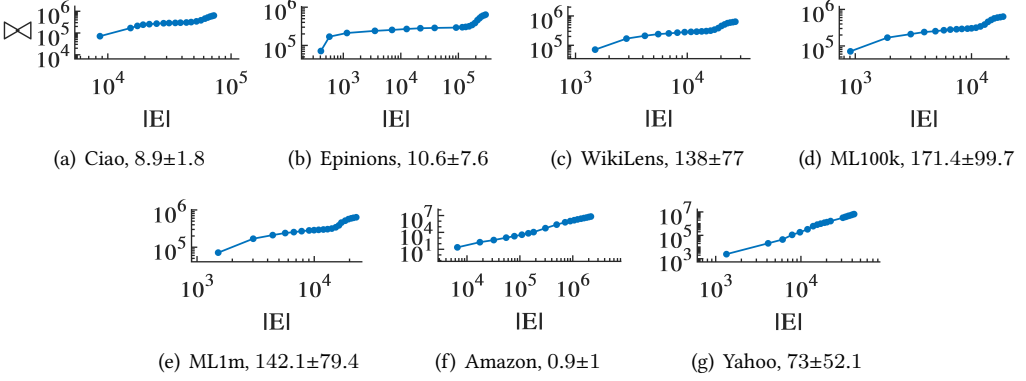


Fig. 2. Butterfly count versus edge count in real-world streams with various average butterfly rates.

$Pr(\delta)$ for all graphs is heavier in the region $[\mu_\delta, \mu_\delta + \sigma_\delta]$ with probability of $Pr(\mu_\delta < \delta \leq \mu_\delta + \sigma_\delta) \approx 0.25$ (according to F_2 values) and gets lighter at the end. This demonstrates that the majority of butterfly edges are formed by vertices with similar strengths at all time points. Also, the strength assortativity localization factor is $0.15 \leq r^s \leq 0.2$ in all graphs at almost all time points (Figure 4).

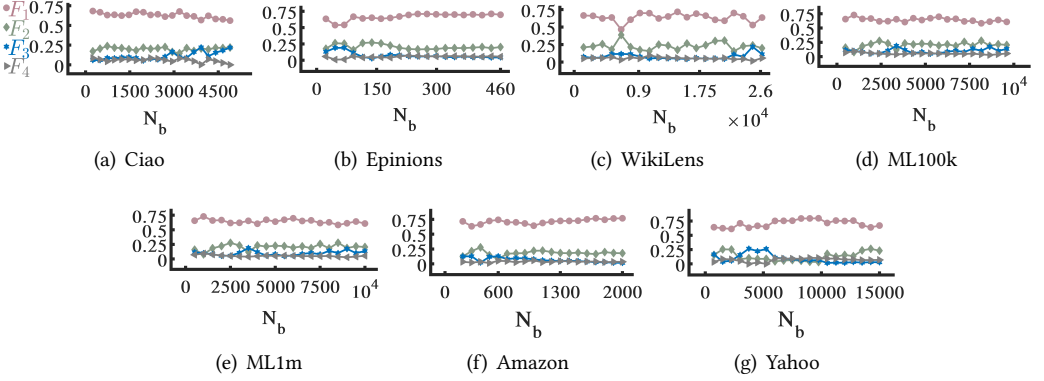


Fig. 3. F elements over the timeline of burst arrivals in real-world streams.

Figure 5 shows the evolution of three statistical quantities for $Pr(\delta)$: (1) mean μ_δ , (2) coefficient of variation $CV = \sigma_\delta / \mu_\delta$, and (3) excess kurtosis $Y_2 = (N^{-1} \sum \delta_i (\delta_i - \mu_\delta)^4 / \sigma_\delta^4) - 3$. Figure 6 shows the evolution of the same quantities for $Pr(S_i)$ and $Pr(S_j)$. CV , also known as relative standard deviation (RSD), enables measuring the degree of variation (dispersion) over distributions with different mean values. A high-variance distribution has $CV > 1$ and a low-variance distribution has $CV < 1$. Distributions such as exponential distribution with equal mean and standard deviation have $CV = 1$. The excess kurtosis Y_2 enables measuring the heaviness of the tail of distribution relative to a normal distribution (which has $Y_2 = 3$). A heavy-tailed distribution has a positive Y_2 (called a *leptokurtic* distribution) and a light-tailed distribution has a negative Y_2 (called a *platykurtic* distribution). Distributions such as family of normal distributions have zero Y_2 (called *mesokurtic*). We observe that the mean and standard deviation of strength-differences are equal to each other and evolve synchronously (Figure 5 – $CV \approx 1$ for sequential G_{N_b}). On the other hand, the tail of right-skewed

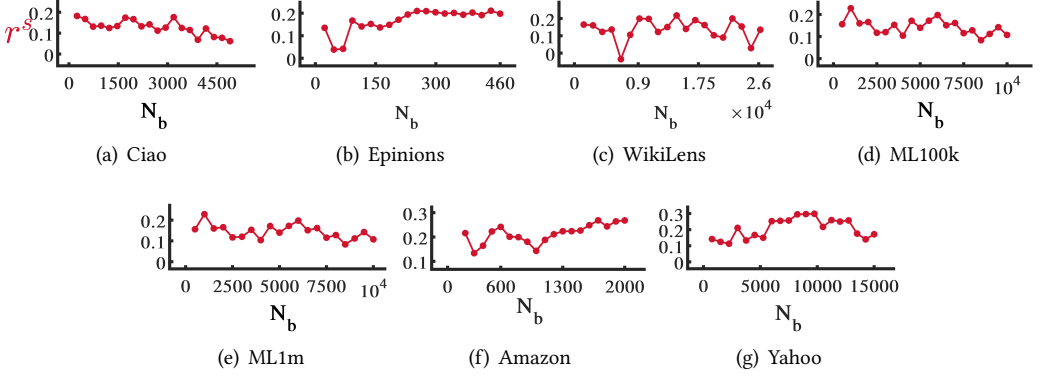


Fig. 4. Strength assortativity localization factor (r^s) of butterflies over the timeline of burst arrivals in real-world streams.

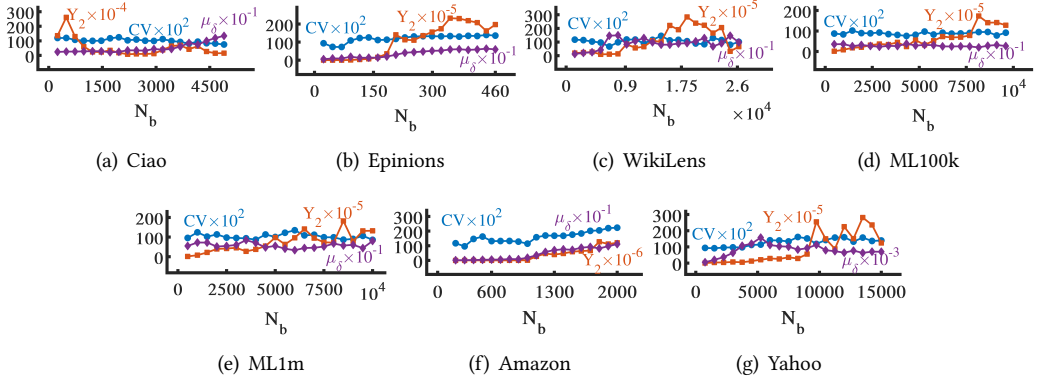


Fig. 5. Coefficient of variation (circles), excess kurtosis (squares), and mean (diamonds) of butterfly strength-differences over the timeline of burst arrivals in real-world streams.

$Pr(\delta)$ gets heavier and the distribution gets broader (Figure 5 – Y_2 increases). In Ciao, the tail gets lighter initially and then gets heavier. Moreover, We observe that all of the graphs have right-skewed $Pr(S)$ which gets broader and more skewed over time with the tail of strength distribution becomes heavier/longer over time (Figure 6 – Y_2 and $CV > 1$ increase). These observations make the steady behavior of strength assortativity more interesting; despite the fact that new high-strength vertices form butterflies and $Pr(\delta)$ gets broader, the relative standard deviation of δ s does not change significantly and the strength assortativity localization factor r^s remains steadily positive. This implies that these graphs obey non-trivial mixing patterns. Understanding these mixing patterns relies on studying the connection micro-mechanics responsible for generating the graphs. Therefore, in the following, we study the growth mechanisms using synthetic graphs and investigate their properties with respect to the observed patterns.

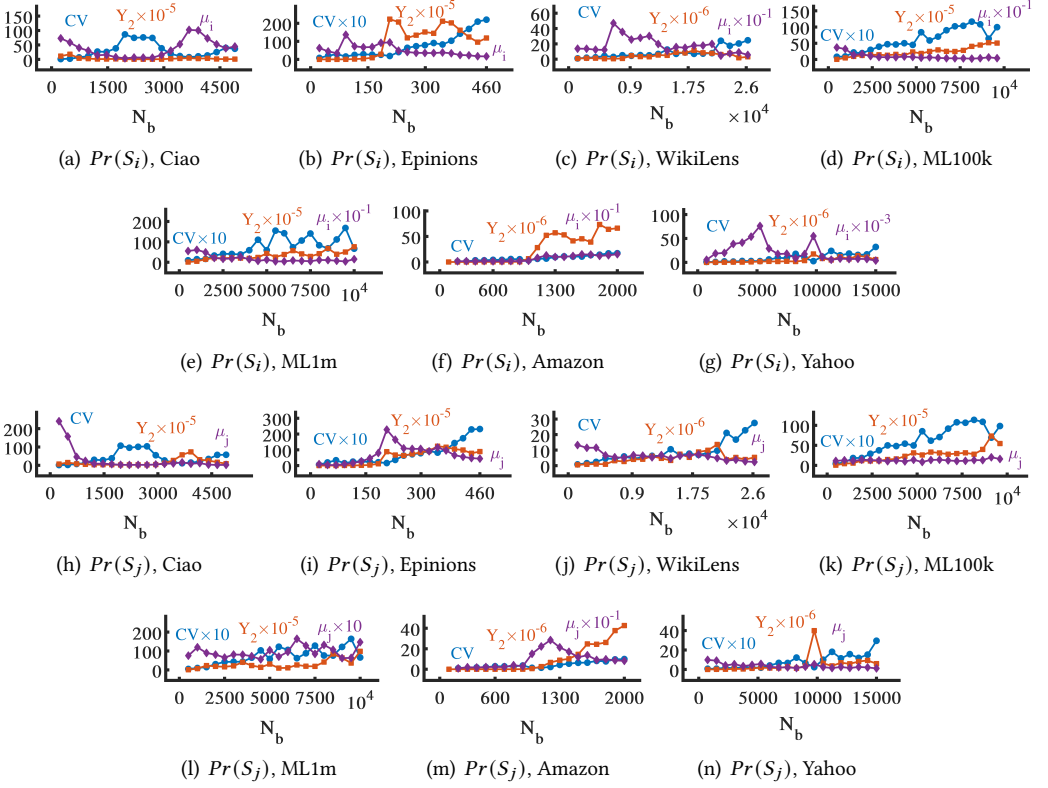


Fig. 6. Coefficient of variation (circles), excess kurtosis (squares), and mean (diamonds) of strengths of butterfly (a-g) i-vertices and (h-n) j-vertices over the timeline of burst arrivals in real-world streams.

4.2 Related Works on Modeling of Graph Patterns - A Brief Survey

The graph models providing micro-mechanics or high-order generative process of graph structure are generally deemed as the explanation for the patterns observed in real-world graphs [13, 33, 69]. We review the graph patterns and the mechanisms used in different graph models to explain the patterns. Our goal is to identify the potential *local rules* [111] (attachment mechanisms based on connections to vertices and their neighborhoods) that explain the observed patterns in previous section. Therefore, we focus on growth models that lead to skewed distributions, degree correlation, and emergence of large numbers of cliques. In the next subsection, we analyze the synthetic streams based on candidate mechanisms to check whether they explain the observed realistic patterns. Our work deviates from the graph models optimized based on downstream analytics task (e.g. link prediction and node classification) and randomizing of the structures in which vertices are associated with feature vectors [112, 126] and also null (feature-driven) graph models [107] generating prescribed patterns/features such as degree-wise metamorphosis coefficient [6], degree distribution [6, 38, 86, 101], subgraph distribution [116], and k-core sequence [107]. We refer to [24, 33] and references therein for surveys of these graph models.

Table 3. Graph Patterns. CC and PL refer to clustering coefficient and power law, respectively.

Patterns	Granularity	Dynamism	References
Small diameter & High CC	Macroscopic	Static	[115]
Degree Correlation	Microscopic	Static	[84]
Community structure	Mesoscopic	Static	[41]
Degree Distribution PL	Microscopic	Static	[14]
Weight PL	Microscopic	Static	[80]
Snapshot/Vertex Strength PL	Mesoscopic	Static	[17, 80]
Gelling points	Macroscopic	Dynamic	[80]
Increasing Average Degree	Microscopic	Dynamic	[70, 71]
Shrinking/Controlled Diameter	Macroscopic	Dynamic	[37, 70, 71]
Edge Densification	Microscopic	Dynamic	[70, 71]
Bursty Weight Addition	Microscopic	Dynamic	[80]

Graph Patterns. Graph patterns characterize a microscopic, mesoscopic, or macroscopic property of a graph (depending on the granularity of the reporting pattern, i.e. vertices/edges, neighborhoods and motifs, or the entire topology) and can be viewed as either static or dynamic (depending on the underlying graph being a static snapshot or an evolving structure). Examples of static patterns include small diameter accompanied by high clustering coefficient [115], degree (anti)correlation [84], community structure [41], and power-laws (PL) such as degree distribution PL [14], weight PL [80], and snapshot/vertex strength PL [17, 80]. Examples of dynamic patterns include gelling points [80], increasing average degree, shrinking/controlled diameter, edge densification [37, 70, 71], and bursty weight addition [80]. Table 3 provides instances of different patterns partitioned across dynamism and granularity.

Growth Models. Two well-studied network growth mechanisms, preferential attachment and copying, form the basis of many generative models [2, 13, 20, 27, 30, 47, 50, 64, 66, 92] and are widely adopted in development of graph management approaches [25, 56, 60, 76, 79, 82, 119]. Both mechanisms are commonly applied in graph models based on the conception of adding a new vertex at each time step during an iterative process. Preferential attachment leads to skewed distributions, while copying mechanism leads to degree correlation [111] and emergence of large numbers of cliques when applied explicitly [66] or implicitly and among other mechanisms [70]. In the following, we review these mechanisms and their alternatives and extensions.

Barabasi-Albert model [14] starts with a small clique with m_0 vertices and applies the preferential attachment by connecting the new vertex to $m \leq m_0$ existing vertices selected randomly with probability proportional to their degrees. The preferential attachment rule has also been extended to strength-driven preferential attachment (SPA) where each new vertex is connected to m existing vertices randomly selected with probability proportional to their strength [17, 18, 72]. It has been shown that preferential attachment is induced by the following microscopic mechanisms. All of these mechanisms imply that the probability that a vertex receives a new edge is proportional to its degree, therefore they amount to preferential attachment and lead to scale-free structures [8].

- Copying [62, 66]: at every time step, a new vertex is connected to a constant number of vertices and the end point of each new edge is a randomly selected vertex with probability p or a neighbor of a prototype vertex with probability $1-p$.
- Edge redirection [65]: at every time step, a new vertex is added and a directed edge from the new vertex to a randomly selected vertex is created with probability $1-p$, or the edge is redirected to the ancestor of the randomly selected vertex with probability p .

- Random walks [110]: at every time step, a new vertex is connected a random vertex and the vertices reachable from it through breadth-first traversal with probability p until no new target is found.
- Attaching to edges [32]: at every time step, a new vertex is connected to two connected vertices.

The original version of copying, mentioned above, copies a neighbor of a randomly selected vertex with some probability at each time step. Other works have modified it as the following.

- Butterfly model [80] mixes copying and random walk mechanisms: at every time step, with probability p_{host} a new vertex picks a random vertex called host and with probability p_{link} forms edges with the vertices reachable from the host through a probabilistic random walk with traversal probability p_{step} . This model exhibits shrinking diameter, stabilized next-largest weakly connected component size, and edge densification.
- Growing network model with copying [64] connects the new vertex to a randomly selected vertex as well as its neighbors which leads to sparse ultrasmall graphs with logarithmic growth of the average degree wrt the number of vertices while the diameter equals 2.
- Duplication divergence model [111] removes the copied neighbors with some probability leading to power law decay of clustering coefficient as a function of degree.
- Nearest neighbors model [111] connects the new vertex to one randomly selected vertex and copies one neighbor with some probability leading to clustering coefficient power law and correlation between average neighbor degree and vertex degree.
- Forest Fire model [70, 71] applies the copying process by recursively, connecting each new vertex to a randomly selected vertex and certain numbers of its randomly selected out- and in-neighbors with forward probability p and backward probability p_b . This process leads to heavy-tailed in- and out-degree distributions due to an implicit preferential attachment, community structures due to neighbor copying mechanism [17], edge densification due to many internal-edge establishments, and shrinking diameter due to shortcut-edge establishments.

Our Work. We identify/explain mesoscopic dynamic patterns in weighted bipartite streaming graphs. To apply the local rules in which new vertices connect to target vertices and their neighbors, it is important to decide when and how many target vertices are selected, how to select the target vertices, and how to copy their neighbors. As we will discuss in the next section, in our growth model, we perform a preferential random walk (PRW) with a dynamic and randomized length bounded to a parameterized range and combined BFS and DFS traversals. We use this PRW as a backbone including the target i - and j -vertices. That is, the number of target vertices in each iteration is non-static and the target vertices are selected via strength-driven preferential method. Given a new edge between v_i and v_j , we connect each target i -vertex u_i to v_j and we copy each u_i 's neighbor as a neighbor of v_i , with a parameterized probability ρ . We also connect each u_i to a j -vertex z_j selected uniformly at random. We perform this procedure for target j -vertices as well. This procedure is done during a burst addition mechanism in which a batch of new isolated edges with a randomized size m , bounded to a parameter value, are added to the graph. This burst addition adds burst per new vertex and per iteration. We further optimize the burst addition mechanism with realistic assignment of weights and timestamps to the edges to ensure realistic connection iterations. We also enforce a time-based filtering on the neighborhoods by using a sliding window over the computational graph.

4.3 Analysis of Microscopic Growth Mechanisms

As we discussed above, preferential attachment leads to skewed distributions, and copying mechanism (particularly with the implementation scheme of Forest Fire model) leads to degree correlation

and emergence of cliques and edge densification as well. Therefore, in an attempt to explain the origins of the observed patterns in real-world streams, we investigate the properties of synthetic graph streams generated by these local rules. We synthesize weighted bipartite streaming graphs such that the graph structure grows according to the Forest Fire (FF) and strength preferential attachment (SPA) models. To this end, we create directed graphs via the growth models and treat the source vertices as the i -vertices and destination vertices as the j -vertices. For the timestamp assignment, we use the time step at which new vertices are connected to existing vertices and for the weight assignments, we use random integers in the range $[1, 5]$ (the same weight scale as in real-world streams). In Forest Fire model, when the backward-burning probability p_b is fixed and the forward-burning probability p increases, the graphs become denser and more clique-like with low diameter [71]. Therefore, we generated graphs with fixed $p_b = 0.3$ and $p = 0.15$ (sparse region), 0.4 (transition region), and 0.7 (dense region). Our experiments show that most of the edges are burned (visited) after checking the neighbors of the ambassador vertex, therefore we do not check further edges to reduce computations and also allow addition of new external links beside the internal densification. In the SPA model, we use $m \in \{10, 50, 100\}$ since the average degree of vertices in real-world streams are mostly below 100 (Table 1). We use the same analytical approach as for real-world streams to investigate the emergence patterns of butterflies in the synthetic streams quantitatively (by checking the growth patterns of butterfly count) and qualitatively (by checking the assortativity patterns of butterflies and the confounding distributions).

As shown in Figure 7, the butterfly count has a slow growth in FF streams and a speedy growth in SPA streams. The average butterfly rate is less than 1 in FF streams and higher than 500 in SPA streams. That is, the growth of butterfly count with respect to the number of edges in the sequential graph snapshots is sub-linear in FF streams and extremely super-linear in SPA streams.

Figure 8 shows the evolution of r^s and the corresponding F elements for the three parameter regions in FF streams. As the graph grows, in the transition region, the assortativity level fluctuates, and, in the sparse and dense regions, it changes trivially (0.02). We check the statistics of the corresponding $Pr(\delta)$ s in Figure 9 and that of $Pr(S_i)$ s and $Pr(S_j)$ s in Figure 10. Although in FF stream butterflies emerge such that the range of $Pr(S_i)$ and $Pr(S_j)$ get broader and more skewed over time, strength-difference of butterfly edges retain the same distribution. $Pr(\delta)$ remains unchanged with a low dispersion ($CV < 1$) as the graph grows in each region since the mean, and standard deviation are fixed and the tail changes slightly over time. Therefore, it is not surprising that r^s is stable. Moreover, in the denser graphs with more butterflies, assortativity patterns vanish ($r^s \rightarrow 0$ as p increase).

Figure 11 shows the evolution of r^s and the corresponding F elements in SPA streams. For small values of m , there is no assortativity pattern. For $m = 100$, the graph snapshots display weak assortativity ($0.05 \leq r^s < 0.1$). We check the statistics of the corresponding $Pr(\delta)$ s in Figure 12 and that of $Pr(S_i)$ s and $Pr(S_j)$ s in Figure 13. As the graph grows, for all values of m , diversity of the strength of i - and j -vertices does not change significantly (small change in μ_i , μ_j , and corresponding CV and Y_2). The strength-differences continuously follow a skewed distribution with a short tail as most δ s remain around the mean ($F_1 + F_2 \approx 0.85$ and $CV < 1$) and the skewness does not grow to very high numbers.

4.4 Discussion

We observe the following concurrent mixing patterns held in the real-world streams as butterflies emerge over time:

- \mathfrak{b}_1 Butterfly densification – The number of butterflies grows over time and at each time point it is a super-linear function of the number of edges. This is in line with a previous study [98].

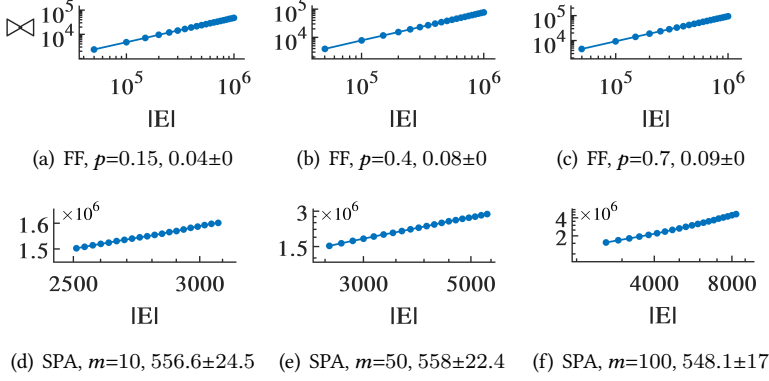


Fig. 7. Butterfly count versus edge count in FF and SPA streams with various average butterfly rates.

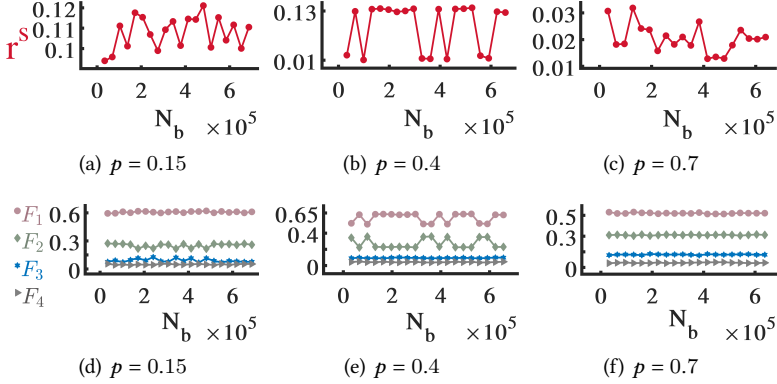


Fig. 8. (a-c) strength assortativity localization factor and (d-f) corresponding F elements of butterflies over the timeline of burst arrivals in FF streams with $p_b = 0.3$, $p = 0.15, 0.4, 0.7$.

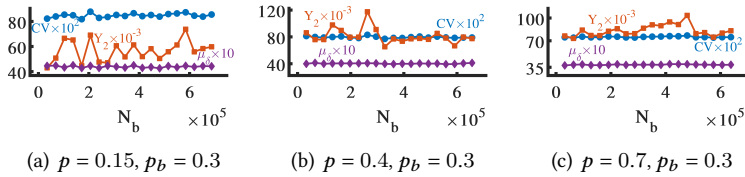


Fig. 9. Coefficient of variation (circles), excess kurtosis (squares), and mean (diamonds) of butterfly strength-differences over the timeline of burst arrivals in FF streams with $p_b = 0.3$, $p = 0.15, 0.4, 0.7$.

p_2 Strength diversification – $Pr(S)$ of butterflies is initially mesokurtic and gets more right-skewed as the right tail grows heavier/longer (Y_2 starts from 0 and rises to extremely high values). The dispersion of strengths increases over time ($CV > 1$ increases) as the standard deviation increases and the mean decreases.

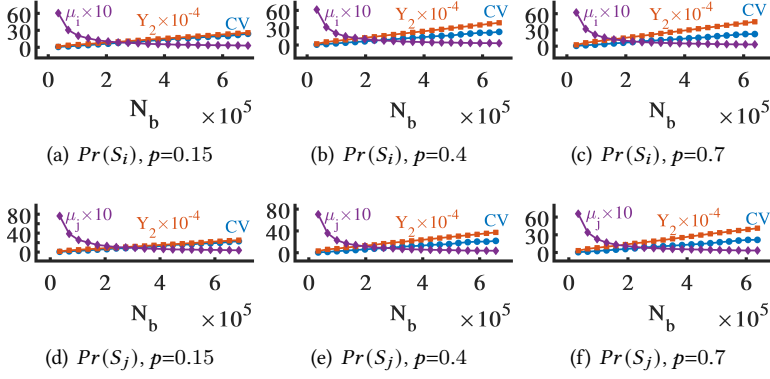


Fig. 10. Coefficient of variation (circles), excess kurtosis (squares), and mean (diamonds) of strengths of butterfly (a-c) i-vertices and (d-f) j-vertices over the timeline of burst arrivals in FF streams with $p_b = 0.3$, $p = 0.15, 0.4, 0.7$.

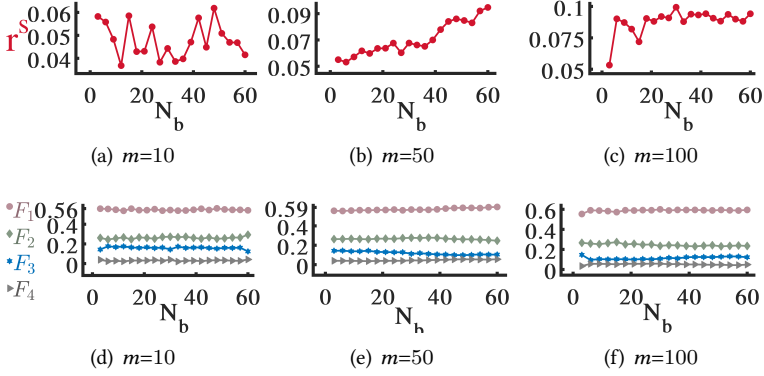


Fig. 11. (a-c) strength assortativity localization factor r^s and (d-f) corresponding F elements of butterflies over the timeline of burst arrivals in SPA model with $m = 10, 50, 100$.

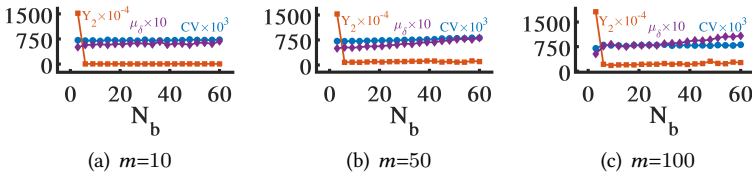


Fig. 12. Coefficient of variation (circles), excess kurtosis (squares), and mean (diamonds) of butterfly strength-differences over the timeline of burst arrivals in SPA model with $m = 10, 50, 100$.

\mathfrak{p}_3 Steady strength assortativity – The strength assortativity localization factor r^s is fixed at a positive value over time due to the fixed-shaped yet growing distribution of strength-differences of butterflies. $Pr(\delta)$ is initially mesokurtic and gets more right-skewed as the

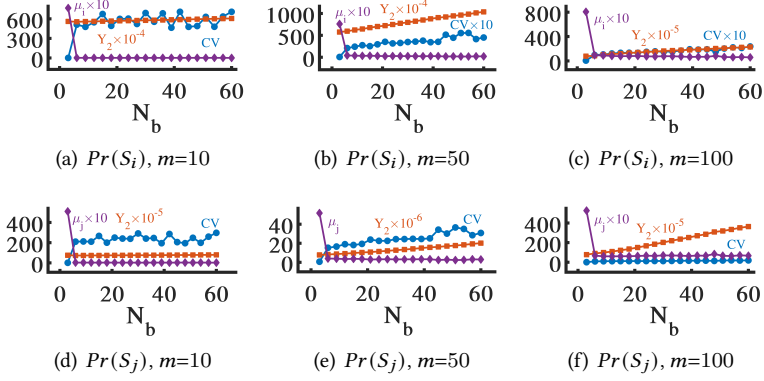


Fig. 13. Coefficient of variation (circles), excess kurtosis (squares), and mean (diamonds) of strengths of butterfly (a-c) i -vertices and (d-f) j -vertices over the timeline of burst arrivals in SPA model with $m = 10, 50, 100$.

right tail grows heavier/longer (Y_2 starts from 0 and rises to extremely high values). However, the dispersion of strength-differences does not change ($CV \approx 1$) due to synchronous evolution of mean and standard deviation. Also, the proportion of δs in different regions of $Pr(\delta)$ is constant (stable F elements). Therefore, the shape of the distribution is stable although the range expands.

The co-occurrence of these patterns is counter-intuitive and interesting. As the stream and the number of butterflies grow rapidly, we observe that diversity of strengths for butterfly vertices increases and strong (high-strength) vertices get stronger and obtain weak neighbors with the increasing of variance of strength differences. Therefore, we expect an increasing trend of disassortativity. However, we observe that the majority of butterfly edges are formed by vertices with similar strength and this assortativity remains at a fixed level regardless of stream size or butterfly count. We refer to this phenomenon as *scale-invariant strength assortativity of streaming butterflies*, which is originated by the three parallel mixing patterns of butterflies.

To explain the data-driven semantics of the observed patterns in the domain of user-item rating streams, we relate them to the following graph concepts:

- **Burstiness** – User-item interactions can be viewed as human-initiated events which introduce two levels of burstiness: individual-level and group-level. The former relates to the interactions of each user with several items at each time point or sequential time points with negligible differences. Such bursty interactions leads to formation of many wedges incident to each user/item. The latter relates to the concurrent interactions of several users at each time point. Such bursty interactions lead to merging the individual-level wedges and densification of butterflies. The significance of this continuous burstiness can change over time due to different circumstances leading to peak hours. For instance, Alibaba has reported that customer purchase activities during a heavy period in 2017 resulted in generation of 320 PB of log data in a six hour period [88].
- **Strong-get-stronger** – Online platforms utilize filters such as trends, best sellers, mostly viewed, hot/top categories, newly added, as well as timely promotions, point collection rewarding strategies, and (advertised) recommendations. These systematically lead to the increasing popularity and visibility of the items with most interactions and encouraging the users to interact more and become more active. Such interaction mechanics are similar to the

rich-gets-richer argument, where the richness denotes the vertex strength. The butterflies are formed incident to such highly connected and high strength users/items (strong vertices) leading to butterfly densification and diversification of strengths.

- Core-periphery – Popular items attract the active users and in another view, active users mostly engage with trending items or make items trending/popular. This is similar to the mesoscale phenomenon core-periphery [28, 54] also called rich club [26, 127] stating that high-degree vertices tend to connect to each other and create a core attracting the new connections. Such core sets of vertices with high degrees/strengths in user-item streams create numerous edges between strong users and items with high butterfly support leading to assortativity patterns of butterfly vertices.

We now discuss the properties of FF and SPA streams with respect to the observed patterns. FF streams follow \mathbf{p}_2 but not \mathbf{p}_1 and \mathbf{p}_3 . In FF streams, as the new vertices attach to random vertices (ambassadors) and reach high-degree vertices (hubs) through copying the neighbors of ambassador, new butterflies emerge and the diversity of strength of butterfly vertices increases. When the probability of neighbor copying p is low (sparse regions), the new vertex establishes fewer connections, therefore, the probability of connecting to the high-strength hubs is lower and also the strength of the new vertex remains low. As a result, many edges have low strength-difference, $Pr(\delta)$ is broader, and strength assortativity localization factor is positive. On the other hand, when p is high, although the number of butterflies is higher, the connections are established between pairs of vertices with both low and high strength-difference since the ambassadors and their neighbors are selected uniformly at random. As a result, $Pr(\delta)$ has a lower variance and the strength assortativity displays randomness. Moreover, the butterfly count is a sub-linear function of the number of edges over time even when the graph displays edge densification (in dense regions). SPA streams follow \mathbf{p}_1 but not \mathbf{p}_2 and \mathbf{p}_3 . In SPA streams, as new low-strength vertices attach to m vertices with the highest strengths (strong vertices), many butterflies are formed around the high-strength vertices with a rate much higher than that of real-world streams. When the number of connections per new vertex m is higher, the probability of attachment to low-strength vertices is higher since the number of strong vertices is limited, therefore the number of edges among low-strength vertices increases. As a result, the graphs display weak strength assortativity when average degree is high. When m is low, the number of edges with high strength-difference is higher compared to the case with high m , although they don't exceed edges with low strength-difference. The diversity of $Pr(S)$ and $Pr(\delta)$ does not increase significantly in either cases.

To summarize, FF streams with implicit degree-driven preferential attachment and neighbor copying yield graphs with increasing diversity of strengths of butterfly vertices, however the quantity of butterflies and their mixing schemes do not preserve realistic patterns. SPA streams with pure strength-driven preferential attachment lead to graphs with rapidly growing butterfly density, however the mixing patterns do not match realistic patterns. This highlights the essence of a growth model which has both strength-driven preferential attachment and neighbor copying flavors to ensure a balanced butterfly densification and incremental strength diversity. Further considerations regarding the integration of these two mechanisms with other effective mechanisms are also required to create realistic streams. We resolve this in the next section.

5 THE PROPOSED STREAMING GROWTH MODEL: sGrow

In the previous section, we identified burstiness, strong-gets-stronger, and core-periphery as the semantic concepts explaining the butterfly emergence patterns and also the strength preferential attachment and neighbor copying as the microscopic mechanisms explaining the butterfly densification and strength diversification. Now, we integrate these concepts and growth mechanisms with

further mechanisms that we introduce in the body of our streaming growth model, called *sGrow*, to explain the co-occurrence of all three realistic emergence patterns of butterflies in streaming graphs such that all four-vertex graphlets emerge in the graph, the sgrs are realistic (i.e. preserve streaming data characteristics), and the stream properties are configurable. Figure 14 illustrates a summary of introduced microscopic mechanisms and the techniques for implementing them.

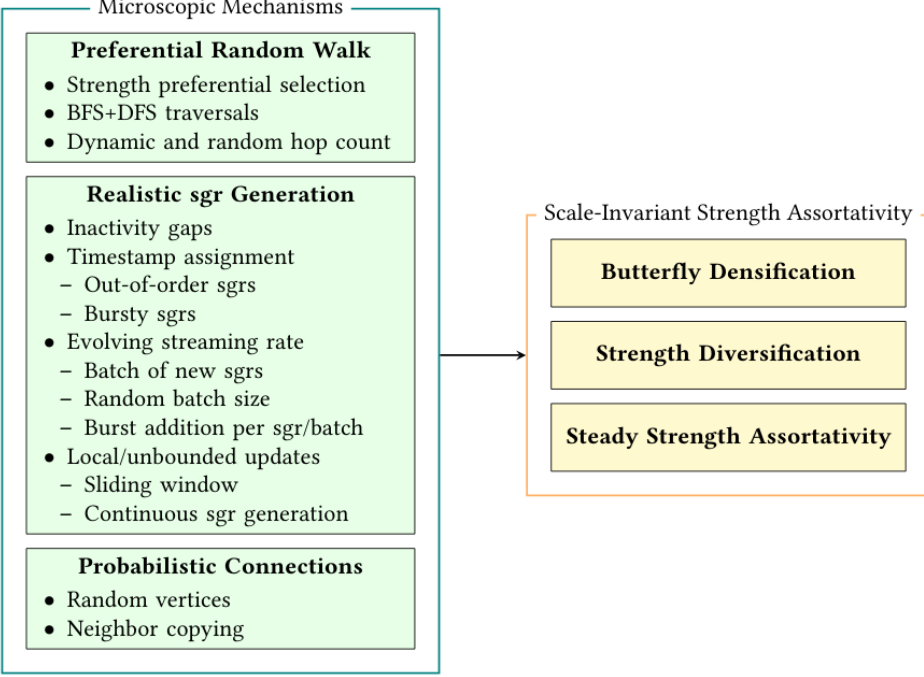


Fig. 14. Introduced microscopic mechanisms and techniques for explaining butterfly emergence patterns.

5.1 Overview

We provide an overview of *ofsGrow* (Algorithm 1 - Figure 15). We use a sliding window mechanism to generate a sequence of *sgrs* that constitute the synthetic *weighted bipartite streaming graph*. In the following G refers to the computational graph snapshot formed by the *sgrs* within the sliding window. The output stream is a sequence of *sgrs* denoted as \mathcal{R} . The time step t , is the computational time point used for controlling the sliding window and the timestamp τ is the *sgr*'s time-label which follows the timestamp scale of an initial graph snapshot. We use five-point scale $[1, 5]$ (similar to that of real-world streams) to generate weights.

G and \mathcal{R} are initiated with an initial graph snapshot $G_0 = (V_0, E_0)$. The sliding window's beginning border W^b is set to the first timestamp in G_0 (lines 1-5 - Figure 15.a). At each time step t , m (a random number in $[0, M]$, where M is a parameter) new *sgrs* $r^{l=1, \dots, m} = \langle v_i^l, v_j^l, \omega_{ij}^l, \tau \rangle$ with new vertices are created and added to \mathcal{R} and G (Figure 15.b,c). The shared timestamp is one plus the last timestamp in G and the weights are random integers $\omega_{ij}^l \in [1, 5]$ (line 8). To connect these new isolated edges to the rest of *sgrs*, the following procedure is followed. A random integer $\omega \in [-1, 5]$ is generated based on which, one of the following three operations is performed for each of the m new *sgrs* in parallel (lines 10-22). Additions and removals happen as described in § 5.2.

- $\omega=-1$, the connection between v_i^l and v_j^l is removed from \mathfrak{R} and G (line 13). This edge removal introduces isolated vertices if the vertices do not acquire neighbors from the current or next batch (v_i^{12} , v_j^{12} , and v_i^{13} in Figure 15.b). Since real-world streaming graphs are dominated by edge additions, we give a lower probability to removals.
- $\omega=0$, nothing happens (line 15). This no-operation introduces a gap of inactivity between streaming records to form **bursts** and also introduces isolated edges. If the current sgr r^l is not connected to the subsequent sgrs in current batch ($r^{l+1, \dots, m}$) or the following batches, it will remain isolated (r^{22} in Figure 15.c).
- $\omega>0$, a j -vertex u_j^0 in G (v_j^{01} in Figure 15.b and v_j^{14} in Figure 15.c) is randomly selected via *Strength Preferential Selection (SPS)* (§ 5.3). Next, a *Preferential Random Walk (PRW)* starting from u_j^0 is performed in G (§ 5.4). The number of hops in PRW (i.e. walk length) is a random integer L in the parameter range $[L_{min}, L_{max}]$. Using this PRW as a backbone, **bursts** of new sgrs between r^l and the rest of sgrs in G and \mathfrak{R} are established (§ 5.5). After adding the last edge with weight ω' , the timestamp τ is incremented as a function of ω' : $\tau=\tau+|(\omega'-5)(\omega'-4)(\omega'-3)/2|$. This function creates a timestamp interval as soon as generation of a sgr with low weight (i.e. $\omega' \leq 2$), therefore it helps characterize the burstiness of the stream (lines 17-22). This is based on an observation in real-world streams that the last sgr in each burst has a low weight. It is noteworthy that there are two level of burstiness: (1) the bursts initiated by each r^l as described here, and (2) the bursts created concurrently by m sgrs $r^{l=1, \dots, m}$ which can be assumed as multiple generative sources.

The aforementioned procedure takes place for all m new sgrs in parallel¹. After that, any newly added vertex with less than two neighbors is removed from G (line 23 - v_i^{22} and v_j^{22} in Figure 15.c). This removal of new isolated vertices is done to retain a connected computational graph, yet the old vertices whose adjacent edges are discarded by the window (as described below) become isolated in G (v_j^{03} in Figure 15.c). Also, the stream may hold isolated vertices/edges (v_i^{22} - v_j^{22} , v_i^{12} , v_j^{12} , and v_i^{13} in Figure 15.c). Next, the timestamp is incremented by one (line 24). The window slides as W^b is incremented by β ; the edges with timestamps out of the sliding window are removed from the graph after each β time steps; and the time step is reset to zero (lines 25-28). This sliding window mechanism is used to avoid pure preferential attachment to old vertices in global scale and create time-sensitive and local connections leading to emergence of young hubs (high degree vertices) to support the observations of real-world stream analysis in [98]. The generation process happens continuously and \mathfrak{R} streams-out as the sgrs are generated. This process can be restricted to continue until a desired number of sgrs S are generated ($|\mathfrak{R}| = S$) and then return the stream \mathfrak{R} .

5.2 Data Structures

We describe the object-oriented data structures and basic graph/stream operators used in the algorithms. A vertex is an object with three attributes: ID, Strength, and timestamp τ . A new $i(j)$ -vertex $v_i(v_j)$ is assigned an integer ID equal to the current number of $i(j)$ -vertices, a strength initialized to zero, and a timestamp equal to that of the edge by which this vertex is added. We use dot notation to refer to attributes of an object, e.g. $v_i.ID$ denotes the ID of the vertex v_i . An edge/**sgr** between vertices v_i and v_j is an object with four attributes: i -vertex (object v_i), j -vertex (object v_j), timestamp (integer τ), and weight (integer ω). The connections of graph G are stored by two hash-map data structures to map each vertex ID to the hash-set of its immediate neighbors: $iNeighbors = \{(v_j.ID : N_i(v_j))\}$ and $jNeighbors = \{(v_i.ID : N_j(v_i))\}$. We use hash-sets since we don't store multiple edges between two vertices in the computational graph and we use hash-map

¹We implemented this algorithm in a single machine shared-memory architecture; a distributed version is doable but not considered in this paper.

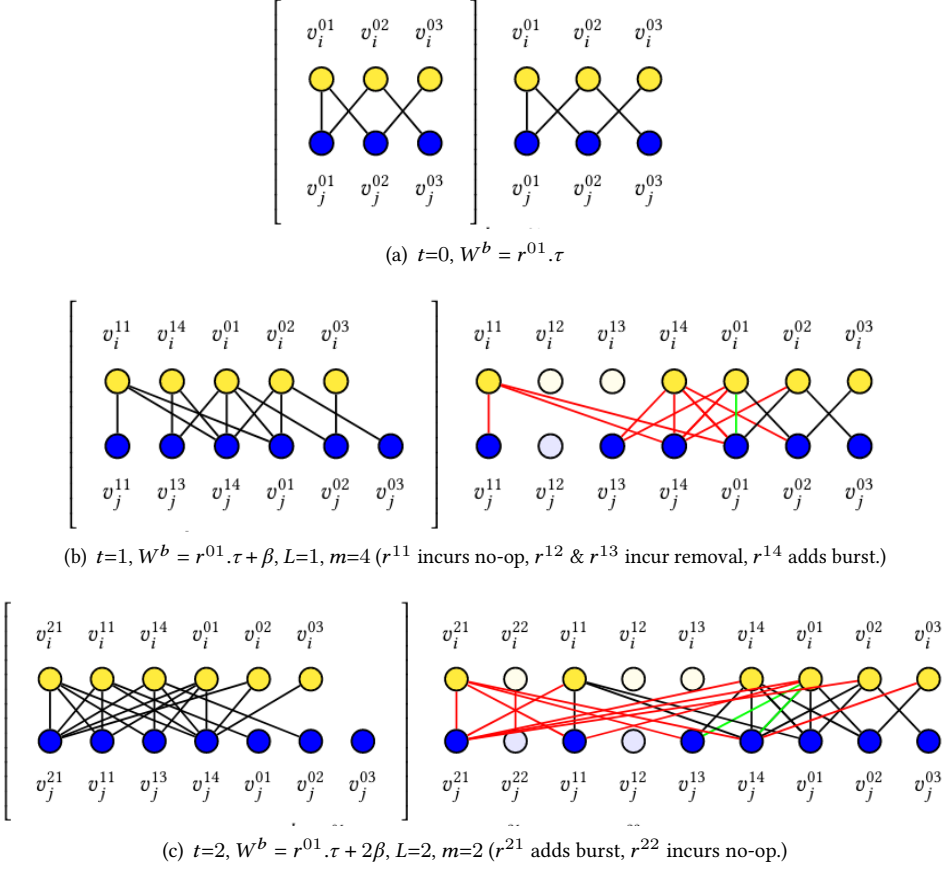


Fig. 15. (left) The computational graph G (right) and the stream \mathfrak{R} at the end of time steps $t=0, 1, 2$ with $\beta=2, \rho=0.4, M=5$, and $L \in [1, 2]$. New edges are in red and PRW edges are in green. (a) At $t=0$, the stream and the computational graph are initiated with G_0 . (b) At $t=1$, a batch of 4 new sgrs ($r^{l=11,12,13,14}$) with same timestamps is created which incur no-op, removal, removal, and burst addition, respectively. v_j^{13} acquires two neighbors after the removal of its connection to v_i^{13} . (c) At $t=2$, a batch of 2 new sgrs ($r^{l=21,22}$) with same timestamps is created which incur burst addition and no-op, respectively. r^{22} does not acquire any neighbor and consequently is removed from G . For simple illustration, we do not depict timestamps and weights in this figure and assume that the edges in G_0 expire from the window as their timestamps are below the W^b .

for fast access to the neighborhoods. The sgrs in \mathfrak{R} are stored in a vector that retains the edges in the order of their additions which include out-of-order sgrs wrt timestamps as we explain in § 5.5. When a new edge is added/removed to/from the graph or stream these data structures are updated accordingly and also the strengths of the vertices at the either ends of the edge are incremented/decremented by the weight of the edge.

5.3 Strength Preferential Selection

We describe function $SPS(V)$ given in Algorithm 2, which is invoked in Algorithms 1 and 3. This function selects a random vertex in the set V according to *strength preferential probability*

Algorithm 1: sGrow

Data: G_0 : an initial graph
Input: ρ : connection probability, M : maximum number of new edges, β : slide parameter, $[L_{min}, L_{max}]$: range of PRW's length
Output: \mathfrak{R} , sequence of streaming graph records

```

1  $G \leftarrow G_0 = (V_0, E_0)$  // computational graph
2  $\mathfrak{R} \leftarrow E_0$  // sequence of sgrs
3  $\tau \leftarrow 1 + \text{last timestamp in } G_0$  // timestamp
4  $t \leftarrow 0$  // time step
5  $W^b \leftarrow \text{first timestamp in } G_0$  // sliding window's beginning border
6 while true do
7    $t \leftarrow t + 1$ 
8   Add  $m \in [0, M)$  new sgrs  $r^{l=1,\dots,m}$  to  $\mathfrak{R}$  and  $G$ 
9   for each  $r^{l=1,\dots,m} = \langle v_i^l, v_j^l, \omega_{ij}^l, \tau \rangle$  do
10      $\omega \leftarrow \text{a random integer in } [-1, 5]$ 
11     switch  $\omega$  do
12       case  $-1$  do
13         Remove  $v_i^l - v_j^l$  from  $\mathfrak{R}$  and  $G$ .
14       case  $0$  do
15         No operation
16       otherwise do
17          $u_j^0 \leftarrow \text{SPS}(V_j)$ 
18          $L \leftarrow \text{a random integer in } [L_{min}, L_{max}]$ 
19          $(PRW_i, PRW_j) \leftarrow \text{PRW}(u_j^0, \text{false}, G, L)$ 
20          $\text{addBurst}(v_i^l, v_j^l, PRW_i, G, \mathfrak{R}, \rho)$ 
21          $\text{addBurst}(v_i^l, v_j^l, PRW_j, G, \mathfrak{R}, \rho)$ 
22          $\tau \leftarrow \tau + \lfloor \frac{(\omega'-5)(\omega'-4)(\omega'-3)}{2} \rfloor$ 
23   Remove any newly added vertex  $v_i^l$  and  $v_j^l$  with less than 2 neighbors from  $G$ 
24    $\tau \leftarrow \tau + 1$ 
25    $W^b \leftarrow W^b + \beta$ 
26   if  $t = \beta$  then
27     Remove any edge with timestamp less than  $W^b$  from  $G$ 
28      $t \leftarrow 0$ 

```

$\Lambda_v = \frac{v.\text{strength}}{\sum_{v' \in V} v'.\text{strength}}$ [17, 18]. Vertices in V are concurrently added to a list with multiplicity equal to their strength (lines 4-6). Next, the list is shuffled (line 7) and a random element v_0 in the list is selected as the output vertex (lines 8-9).

5.4 Preferential Random Walk

We describe function $\text{PRW}(\text{starter}, \text{isI}, G, L)$ given in Algorithm 3. This function performs a random walk with L hops on a graph G . It starts from a *starter* vertex whose type determines a boolean flag *isI* (true when *starter* is an i-vertex and false otherwise). At each hop, a neighbor of the

starter vertex ($u_i \in N_i(\text{starter}), u_j \in N_j(\text{starter})$) is selected via strength preferential selection (invoking $SPS(N_i(\text{starter}))$, $SPS(N_j(\text{starter}))$ – Algorithm 2). The selected neighbor (u_i, u_j) is added to a hash set of unique vertices (PRW_i, PRW_j) and is set as the *starter* vertex. The starter flag is accordingly set and the hop counter is incremented by one (lines 6-10 and 12-16). The next hop starts with the last added vertex. When the current selected neighbor is already in the hash set, if it is the last element, the walk continues to another neighbor of that vertex (in depth traversal) and if it is one of the previously selected vertices other than the last element, the walk continues in breadth traversal. Therefore, the walk is a combination of BFS and DFS with random preferential selection.

5.5 Burst Addition

We describe function $addBurst(v_i^l, v_j^l, PRW_i, G, \mathfrak{R}, \rho)$ given in Algorithm 4. This function adds **bursts** of sgrs to G and \mathfrak{R} based on the i -vertices in the PRW_i and new vertices v_i^l and v_j^l given a probability parameter ρ (Figure 16.a). We follow the same procedure to add bursts with respect to the j -vertices in the PRW_j . As illustrated in Figure 16, considering each i -vertex u_i in the PRW_i , the following connections are established:

- Step 1 An edge between u_i and the newly added v_j^l is formed with the timestamp of v_j^l and a weight $\omega' \in [1, 5]$ (lines 3-4 – Figure 16.b). This edge connects the edge $v_i^l-v_j^l$ to the graph and also leads to emergence of $N_1 + N_2$ caterpillars (solid 3-paths in Figure 16.e,f), where N_1 and N_2 are the number of 1-hop (immediate) and 2-hop neighbors of u_i , respectively.
- Step 2 With probability ρ , an edge between u_i and an existing j -vertex z_j , selected uniformly at random, is formed with timestamp $Min(u_i.\tau, z_j.\tau)$ and a weight $\omega' \in [1, 5]$ (lines 5-8 – Figure 16.c). Using a timestamp other than the current timestamp ($v_j^l.\tau$) introduces out-of-order sgrs (late arrival) since this sgr has a timestamp less than ($v_j^l.\tau$). It also helps balance the burst sizes since the current timestamp is not assigned to all edges in the current time step. This probabilistic edge leads to converting the caterpillars between u_i and z_j into butterflies at the generation time of either vertices (closed 4-path in Figure 16.g).
- Step 3 With probability ρ , an edge between the newly added v_i^l and each u_i 's immediate j -vertex neighbor n_j is concurrently formed with n_j 's timestamp $n_j.\tau$ and a weight $\omega' \in [1, 5]$ (lines 9-12 – Figure 16.d). In other words, each of the adjacent links of u_i is copied with probability ρ . Since $n_j.\tau < v_i^l.\tau$, out-of-order sgrs join previous burst of sgrs with same timestamp (including the sgr incident to n_j). These probabilistic edges lead to converting the N_1 caterpillars emerged in Step 1 into butterflies (closed 4-path in Figure 16.e). We run this step for generating streams with high number of sgrs per burst.

6 EVALUATIONS

In this section, we analyze the computational complexity of *sGrow* and evaluate its performance from three perspectives:

- Computational Complexity (§ 6.1) – We theoretically analyze the computational complexity of *sGrow*.
- Pattern Reproducing (§ 6.2) – We examine the ability of *sGrow* to reproduce the realistic patterns under different levels of burstiness, initial graph snapshots G_0 , and butterfly counts. We create streaming graphs with a prefix of 1000 edges from real-world streams (G_0) and the rest of the stream is synthesized via *sGrow* with various parameter configurations and different number of butterflies. We refer to the generated streams as S- $\{G_0\text{-name}\}$.

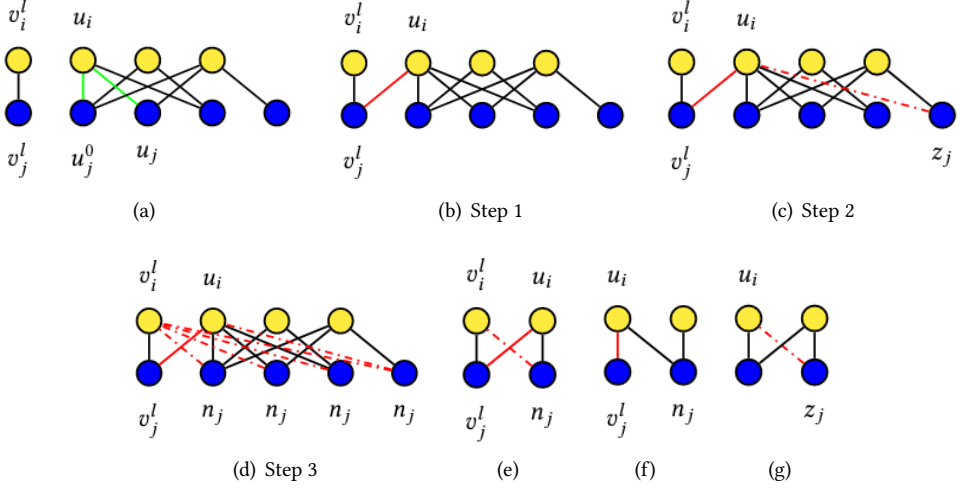


Fig. 16. Four-vertex graphlets (e, f, g) and schematic burst addition steps (b, c, d) based on an i -vertex u_i in the PRW starting from u_j^0 designated by green lines (a). New edges are colored in red and dashed lines denote probabilistic connections.

Algorithm 2: Strength Preferential Selection

```

1 Function  $SPS(V)$ 
2    $list \leftarrow \emptyset$ 
3   for each  $v \in V$  do
4      $S \leftarrow v.strength$ 
5     for  $k=1$  to  $S$  do
6        $list.add(v)$ 
7    $shuffle(list)$ 
8    $index \leftarrow$  a random integer in  $[0, size(list))$ 
9    $v_o \leftarrow list[index]$ 
10  Return  $v_o$ 

```

- Stress Testing (§ 6.3) – We examine the impact of introduced parameterized techniques on the effectiveness, efficiency, and burstiness of the generated stream. We also provide a reference guide for setting the parameters. We use a prefix of 1000 edges from Amazon stream and synthesize the rest of the stream via $sGrow$ with different parameter configurations.

Our experiments as well as the analysis in previous sections are conducted on a machine with 15.6 GB native memory and Intel Core i7–6770HQCPU@2.60GHz*8 processor. We have implemented all algorithms in Java (OpenJDK version 11.0.11).

6.1 Computational Complexity

In the following, we show that high degree/strength vertices and PRW hop count determine the computational expenses of $sGrow$.

Algorithm 3: Preferential Random Walk

```

1 Function  $PRW(starter, isI, G, L)$ 
2    $h \leftarrow 0$  // hop counter
3    $(PRW_i, PRW_j) \leftarrow \emptyset$  // two hash-sets of unique i-vertices and j-vertices of the walk
4   while  $h < L$  do
5     if  $isI$  then
6        $u_j \leftarrow SPS(N_j(starter))$ 
7       Add  $u_j$  to  $PRW_j$ 
8        $starter \leftarrow u_j$ 
9        $isI \leftarrow false$ 
10       $h \leftarrow h + 1$ 
11    else
12       $u_i \leftarrow SPS(N_i(starter))$ 
13      Add  $u_i$  to  $PRW_i$ 
14       $starter \leftarrow u_i$ 
15       $isI \leftarrow true$ 
16       $h \leftarrow h + 1$ 
17  Return  $(PRW_i, PRW_j)$ 

```

Algorithm 4: Add Burst

```

1 Function  $addBurst(v_i^l, v_j^l, PRW_i, G, \mathfrak{R}, \rho)$ 
2   for each  $u_i \in PRW_i$  do
3      $\omega' \leftarrow$  a random integer in  $[1, 5]$ 
4     Add a new sgr  $\langle u_i, v_j^l, \omega', v_j^l.\tau \rangle$  to  $\mathfrak{R}$  and  $G$ 
5     if  $coin(\rho)$  is Head then
6        $z_j \leftarrow$  Select a random j-vertex
7        $\omega' \leftarrow$  a random integer in  $[1, 5]$ 
8       Add a new sgr  $\langle u_i, z_j, \omega', Min(u_i.\tau, z_j.\tau) \rangle$  to  $\mathfrak{R}$  and  $G$ 
9     for each  $n_j \in N_j(u_i)$  do // in highly bursty streams
10      if  $coin(\rho)$  is Head then
11         $\omega' \leftarrow$  a random integer in  $[1, 5]$ 
12        Add a new sgr  $\langle v_i^l, n_j, \omega', n_j.\tau \rangle$  to  $\mathfrak{R}$  and  $G$ 

```

THEOREM 6.1. *The worst case computational complexity of sGrow in each window with graph $G=(V_i \cup V_j, E)$ and PRW parameter L is $O(S_{max} + L(N_{max}^j + N_{max}^i))$, where S_{max} is the maximum strength in G and N_{max}^i and N_{max}^j are the maximum number of i-neighbors and j-neighbors for vertices in V_i and V_j .*

PROOF. sGrow's computations at each window are dominated by burst additions as the initializations, sgr addition/removals, and window sliding take one unit of computation. The worst case computational complexity of burst additions is the following.

$$O(\text{SPS}(.)) + O(\text{PRW}(.)) + O(2\text{addburst}(.)) \quad (5)$$

Let us assume that the maximum strength in $G=(V_i \cup V_j, E)$ is S_{max} , L is the parameter for the PRW hop count, and the maximum number of i -neighbors and j -neighbors for vertices in V_i and V_j are N_{max}^i and N_{max}^j . Accordingly, we would have the following complexities: $O(\text{SPS}(V_j)) = S_{max}$ since the value assignments and corresponding operators, and the list shuffling take one unit of computations, and the outer for loop is parallel and the inner loop sequentially performs S_{max} computational units. We have $O(\text{PRW}(u_j^0, \text{false}, G, L)) = (L/2 + 1)N_{max}^j + (L/2)N_{max}^i$ since $|PRW_j| = L/2 + 1$ and $|PRW_i| = L/2$. Also, $O(\text{addburst}(v_i^l, v_j^l, PRW_j, G, \mathfrak{R}, \rho)) = O(\text{addburst}(v_i^l, v_j^l, PRW_i, G, \mathfrak{R}, \rho)) = O(1)$ since the value assignments, and probabilistic connections are done in $O(1)$ and Step 3 is performed via a parallel loop. Therefore, the total complexity of burst additions would be $S_{max} + (L/2 + 1)N_{max}^j + (L/2)N_{max}^i + O(1)$, i.e. high degree/strength vertices and PRW hop count determine the computational cost. \square

6.2 Pattern Reproducing

As provided in Table 1, Epinions, Amazon, and Ciao are bursty streams with average burst sizes of $b = 27282, 1753.7$, and 14.8 ; Yahoo and ML1m are also bursty but with lower values $b = 2.4$ and 2.2 ; ML100k and WikiLens have the lowest burstiness with $b = 2$ and 1 , respectively. According to these burstiness profiles, we set the parameters to control the temporal distribution of sgrs. That is, to simulate a stream with high burstiness, we set M and $[L_{min}, L_{max}]$ to high values to increase the probability of creating high number of new edges at each timestep (M) and increase the burst size by generating backbone walks with more vertices ($[L_{min}, L_{max}]$). To simulate a stream with low burstiness (S-ML100k and S-WikiLens), we do not perform the neighborhood copying (lines 9-12 in Algorithm 4 – step 3 in § 5.5). The default value of ρ is 0.3 and we further adjust it by decreasing (increasing) to push the burst size towards lower (higher) values. We set $\beta = 5$ in all streams. The exact value of parameters are given in Table 4. All of the reported results in Figures 17-21 are based on the same stream.

Table 4. Parameters

	ρ	M	β	$[L_{min}, L_{max}]$
S-Ciao	0.3	100	5	[2, 3]
S-Epinions	0.2	300	5	[3, 6]
S-WikiLens	0.4	100	5	[1, 3]
S-ML100k	0.3	100	5	[1, 3]
S-ML1m	0.3	10	5	[1, 2]
S-Amazon	0.3	50	5	[1, 2]
S-yahoo	0.3	50	5	[2, 3]

In the following, we compare the synthetic streams generated by *sGrow* and real-world streams with respect to the patterns observed in real-world streams qualitatively by checking whether the patterns hold and quantitatively by checking the error of r^s and F . We observe that *sGrow* streams obey the scale-invariant strength assortativity of butterflies since all the synthetic streams preserve the realistic mixing patterns \mathfrak{p}_1 , \mathfrak{p}_2 , and \mathfrak{p}_3 regardless of the initial graph snapshot, butterfly count, and burstiness level:

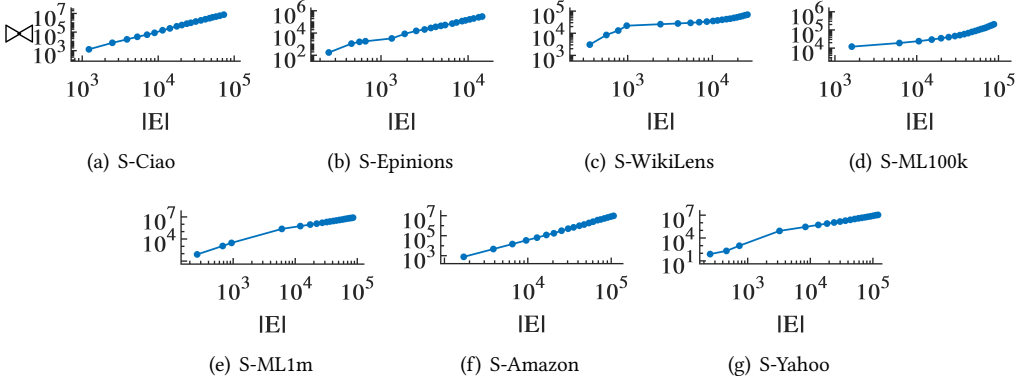
- \mathfrak{p}_1 The number of butterflies grows over time (Figure 17) with an average butterfly rate higher than 1 in all the streams (Table 5) indicating that the butterfly count grows super-linearly with respect to the number of edges .

Table 5. Average butterfly rate in synthetic streams generated by our model.

	average butterfly rate	$ E^{20} $	N_b^{20}	\bowtie^{20}
S-Ciao	37.2440 ± 31.4987	72,966	940	7,430,097
S-Epinions	9.4358 ± 6.1519	14,495	300	304,417
S-WikiLens	6.3037 ± 5.6897	25,957	4,000	69,302
S-ML100k	2.191 ± 1.3045	87,951	12,000	204,118
S-ML1m	59.8963 ± 29.2066	85,397	2,000	7,860,689
S-Amazon	30.8994 ± 28.8517	106,714	4,000	9,599,739
S-Yahoo	51.1708 ± 27.891	120,616	3,200	10,847,746

- \mathfrak{b}_2 The mean, relative standard deviation, and tail skewness/heaviness of $Pr(S)$ increases over time (Figure 18) showing that butterfly vertex strengths diversify over time.
- \mathfrak{b}_3 The synchronous evolution of mean and standard deviation accompanied by increasing skewness/heaviness of the tail of $Pr(\delta)$ (Figure 19) plus the stable values of F elements over time (Figure 20) demonstrate that $Pr(\delta)$ is fixed-shaped yet growing. Moreover, the strength assortativity localization factor changes trivially over time and is positive (Figure 21) with F_1 values between 0.5 and 0.7 indicating the steady strength-assortativity of butterflies over time.

Table 6 presents the mean absolute error of r^s and F elements in *sGrow* streams with respect to that of real-world streams over the sequential burst-based graph snapshots (comparing Figures 4 and 21). We observe that in all synthetic streams the error is between 0.01 and 0.1. This indicates that *sGrow* reproduces the similar strength difference distribution and strength assortativity of butterfly edges as in the real-world streams.

Fig. 17. The number of butterflies \bowtie versus the number of edges $|E|$.

6.3 Stress testing

We evaluate the impact of *sGrow* techniques (batch of isolated edges, probabilistic connections, the random walk backbone, and the sliding window) as the following:

- We use a diverse range of parameters $M \in \{100, 150, 200, 250, 300\}$, $\rho \in \{0.3, 0.4, 0.5, 0.6, 0.7\}$, $L_{min} \in \{1, 2, 3, 4\}$, $L_{max} \in \{3, 4, 5\}$, and $\beta \in \{5, 10, 15, 20\}$ to create S-Amazon stream with initial prefix of 10^3 sgrs from the Amazon stream. In each row of Tables 7, 8, and 9, we

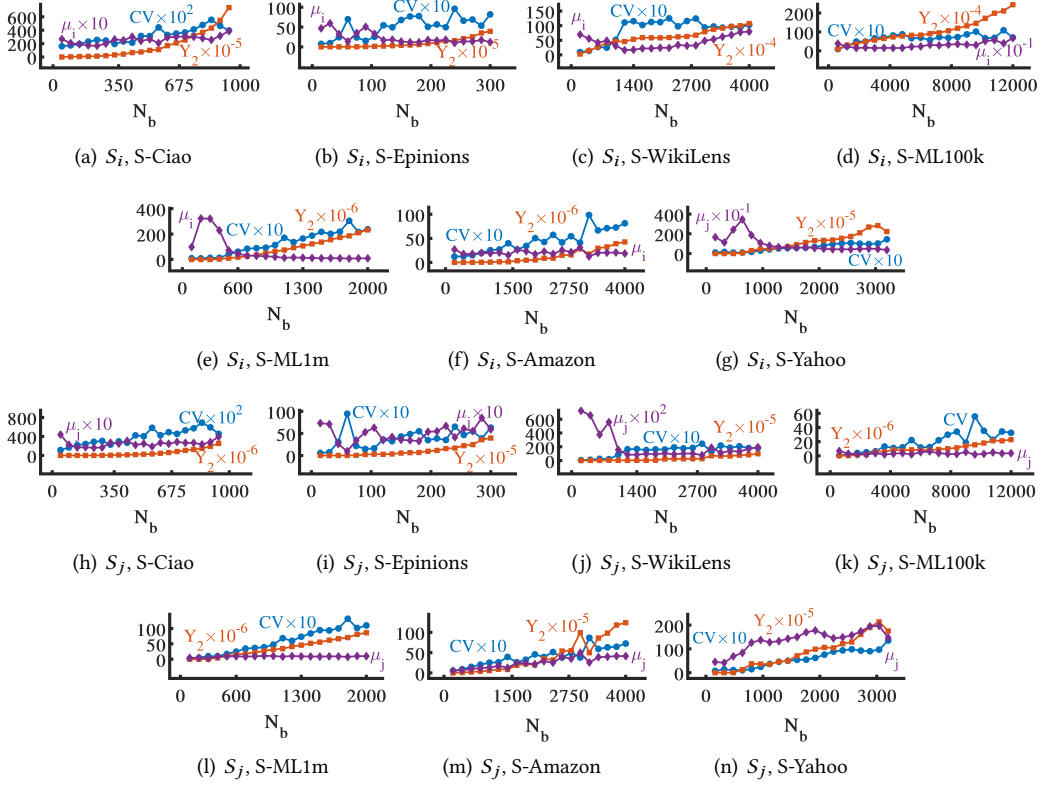


Fig. 18. Coefficient of variation (circles), excess kurtosis (squares), and mean (diamonds) of strengths of butterfly (a-g) i-vertices and (h-n) j-vertices over the timeline of burst arrivals.

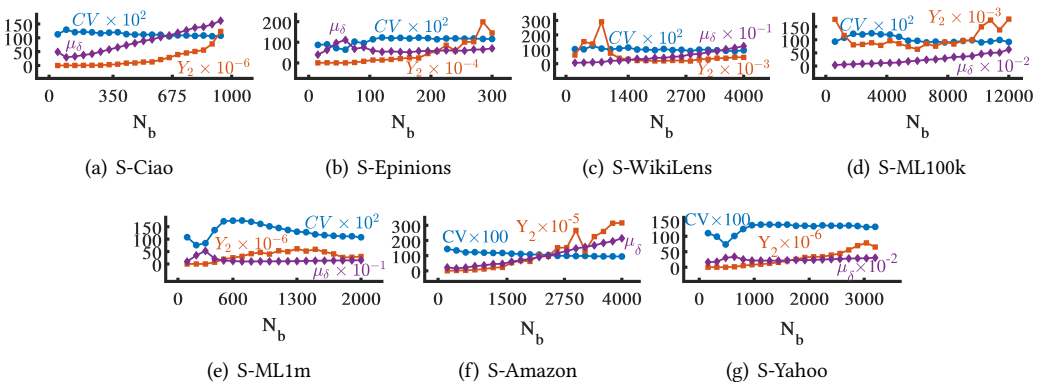


Fig. 19. Coefficient of variation CV (circles), excess kurtosis Y_2 (squares), and mean μ_δ (diamonds) of butterfly strength differences over the timeline of burst arrivals.

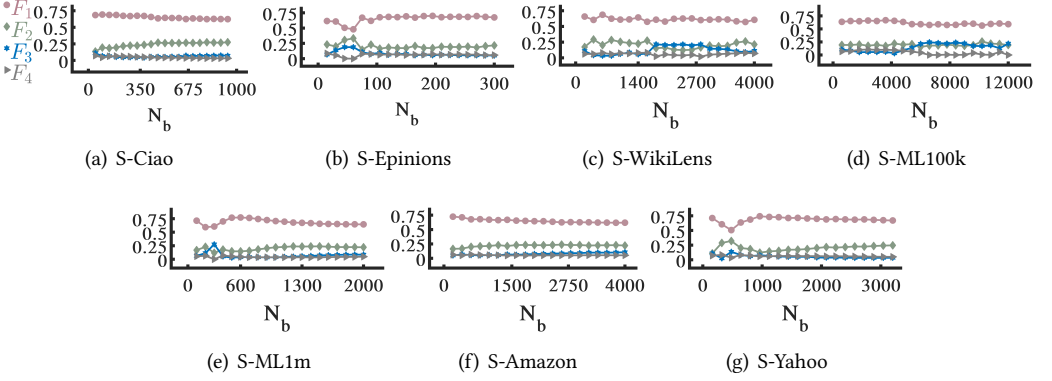
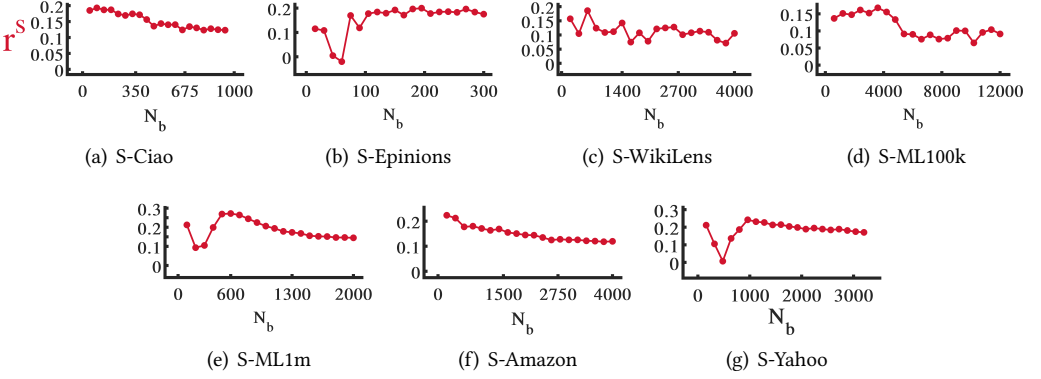


Fig. 20. F elements over the timeline of burst arrivals.

Fig. 21. Strength assortativity localization factor r^s of butterfly vertices over the timeline of burst arrivals.Table 6. Mean absolute error of r^s and F elements.

	F_1, r^s	F_2	F_3	F_4
S-Ciao	0.0286	0.05	0.0569	0.0199
S-Epinions	0.0318	0.0389	0.0219	0.0163
S-wikiLens	0.0528	0.0705	0.08	0.0194
S-ML100k	0.0376	0.0513	0.0642	0.0384
S-ML1m	0.0617	0.0445	0.049	0.015
S-Amazon	0.1064	0.0539	0.0476	0.094
S-Yahoo	0.0578	0.0782	0.0519	0.0316

examine the effect of one parameter on effectiveness, efficiency, and frequency distribution of burst sizes, respectively.

- We also create S-Amazon stream with 10^7 sgrs such that after generating 5×10^6 , one of the parameters switches from $M = 100, \beta = 5, L \in [15]$ and $\rho = 0.4$ to $M = 300, \beta = 20, L \in [45]$ and $\rho = 0.8$. In Figure 22, we examine the effect of the parameter switch on effectiveness and efficiency.

6.3.1 Effectiveness. In Table 7, we check the evolution of r^s as the number of butterflies grows to 10^7 in S-Amazon stream with different parameter configurations. We observe that data points are not clustered by colors (corresponding parameters $[L_{min}, L_{max}]$, M , and β) in rows a, c, and d, however they are clustered and ordered by ρ . Also, $0.1 \leq r^s \leq 0.15$ regardless of $[L_{min}, L_{max}]$, M , and β . The value of r^s is stable at a positive value, which is higher for lower connection probabilities ρ . As the connection probability ρ increases, the probability of establishing connections between the newly added vertices with low strength and high strength neighbors of the PRW vertices increases, therefore the assortativity level decreases. In Figure 22, we check the evolution of r^s as the number of butterflies grows to 10^7 in S-Amazon stream with parameter switch in the middle of stream generation. We observe that compared to the stream with static parameters, the data points of streams with dynamic parameters follow the same pattern after the switch of $[L_{min}, L_{max}]$, M , and β . Increasing the value of ρ slightly decreases r^s , yet the steady state is retained after the switch.

6.3.2 Efficiency. In Table 8, we check the time for generation as the stream grows to 10^7 sgrs in S-Amazon stream with different parameter configurations. We observe that data points are not clustered by colors (corresponding parameters $[L_{min}, L_{max}]$, M , and β) in rows a, c, and d, however they are clustered by ρ and ordered by both ρ and $[L_{min}, L_{max}]$. That is, the generation time is not impacted by M (Table 8.c) or β (Table 8.d), however it is affected by ρ and $[L_{min}, L_{max}]$. As the connection probability ρ increases, the generation time decreases since the number and the size of bursts created at each time step increases (Table 8.b). As the range of random walk length $L \in [L_{min}, L_{max}]$ increases, the generation time decreases since the size of bursts created at each time step increases (Table 8.a). In Figure 22, we check the time for generation as the stream grows to 10^7 sgrs in S-Amazon stream with parameter switch in the middle of stream generation. We observe that switching M and β gradually decreases the slope of generation time curve, while switching L and ρ promptly and significantly changes the slope. This confirms that L and ρ significantly determine the generation time.

6.3.3 Burst Size. In Table 9, we check the frequency distribution of all burst sizes in S-Amazon with 10^7 sgrs generated by different parameter configurations. We observe that for all values of ρ and L_{max} by increasing M , the range of burst sizes expands, therefore M significantly impacts burst sizes. Also, the maximum burst size increases as ρ and L_{max} increase.

6.3.4 Parameter Configuration. The introduced techniques with configurable parameters enable generating realistic bipartite streaming graphs with generation time sub-linear with respect to the number of sgrs. The burstier the stream, the lower the generation time. In the following we elaborate a reference guide for configuring the parameters.

M – The upper bound for the random number of new batched sgrs added at each timestep does not impact the strength assortativity patterns and the generation time. This parameter can be comfortably used to adjust the level of burstiness of the streaming graph without affecting the performance of the generative algorithm.

ρ – The probability of creating an edge between each random walk vertex and a random vertex or an edge between each new sgr and neighbors of the random walk vertices impacts the level of strength assortativity but not its steady state. It also affects the generation time. This parameter can be used to trade off scalability and the level of strength assortativity. The default value is $\rho = 0.3$, yet increasing ρ would decrease the generation time and strength assortativity level. Values less than or equal to 0.7 ensure positive strength assortativity. Also, ρ determines the probability of out-of-order sgrs.

$[L_{min}, L_{max}]$ – The range for random length of PRW backbone used for establishing burst of sgrs does not impact the strength assortativity patterns. It affects the generation time. This parameter can be used to increase the scalability of the stream generation. The default range is $[1, 2]$ and shifting/expanding the range by increasing the lower or upper bound would decrease the generation time.

β – The sliding window parameter used as the frequency and the size of sliding does not impact the strength assortativity patterns and generation time. This parameter can be comfortably used for creating streams in which sgrs are semantically time-sensitive and need a user-specified slide parameter. The default value is $\beta = 5$, while any other value can be set.

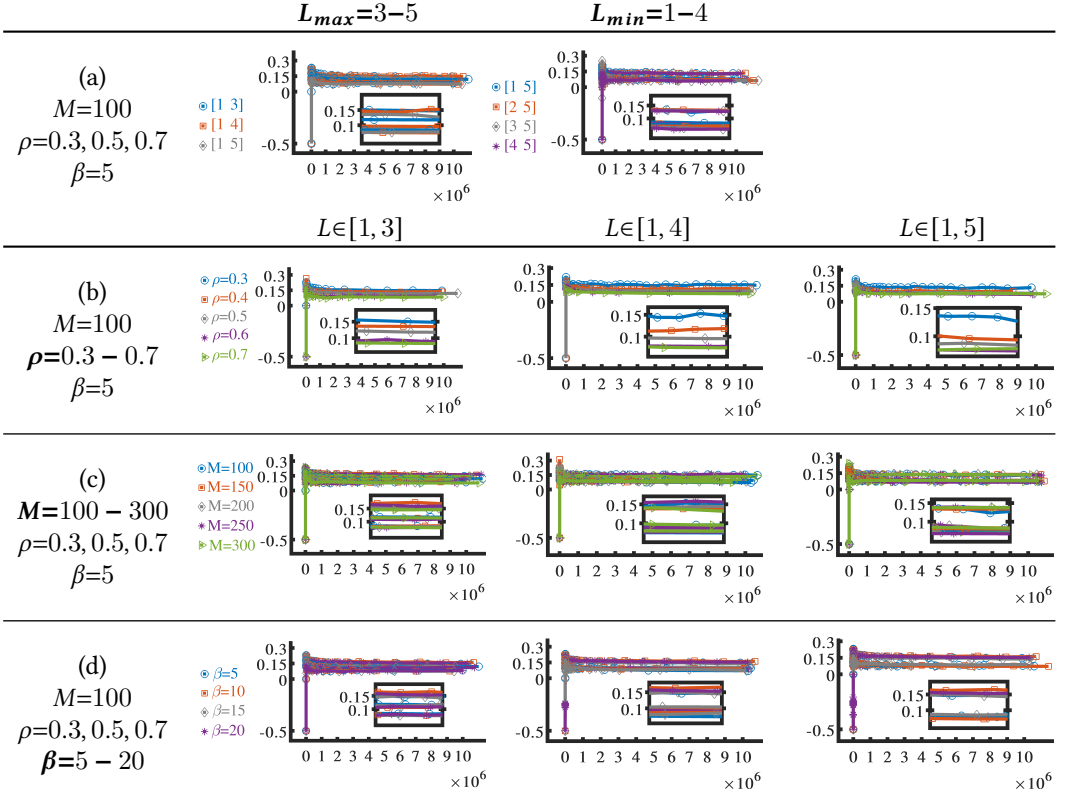
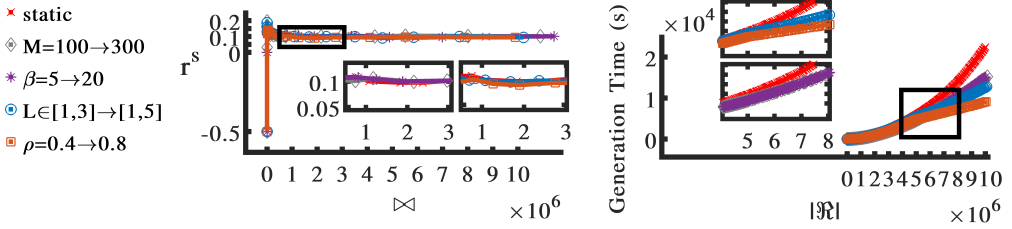
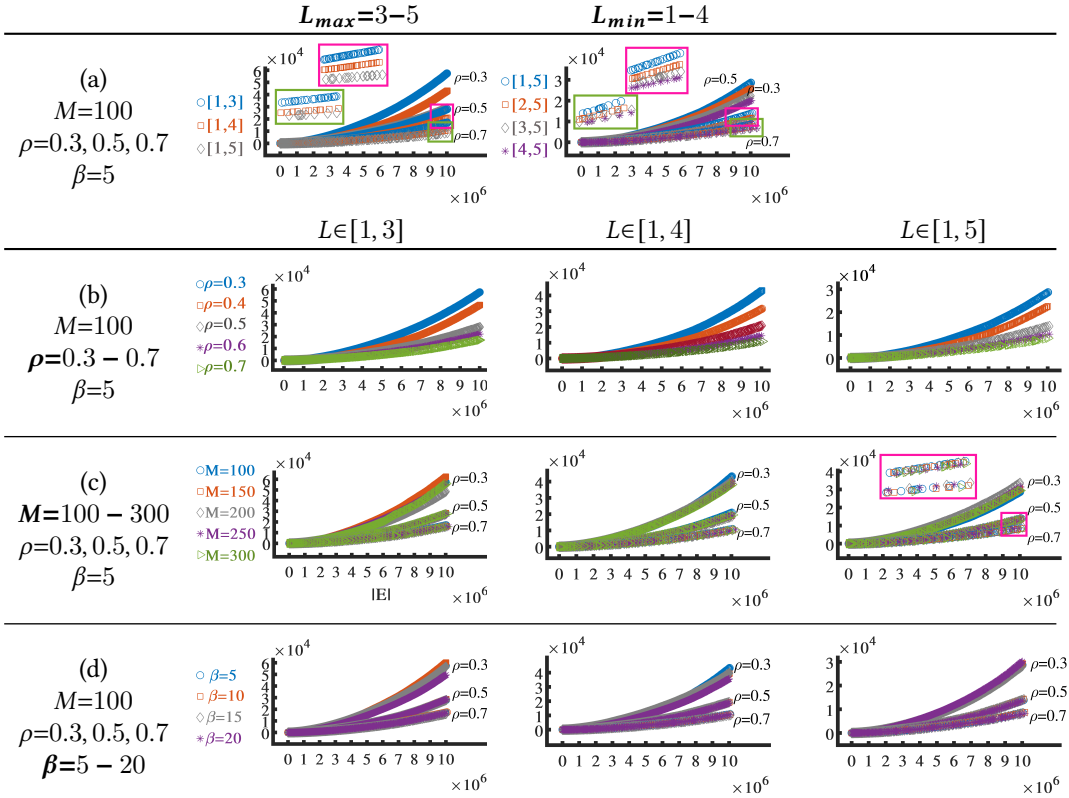


Table 7. Strength assortativity localization factor r^s of sGrow (y axes) versus butterfly count \bowtie (x axes) for S-Amazon with different parameter configurations.

6.4 Discussion

Our evaluations indicate that *sGrow* efficiently and effectively reproduces the bursty emergence patterns of cohesive building blocks in the bipartite streaming graphs, regardless of the initial conditions, the scale and temporal characteristics of the generated stream, and the model configurations. This confirms that the introduced microscopic mechanisms in the body of *sGrow* *robustly* explain the observed streaming growth phenomenon in real-world streams. Our analysis also verifies the ability of *sGrow* in generating realistic streaming graphs configured with user-specified properties



for the scale and burstiness of the stream, level of strength assortativity, probability of-of-order streaming records, generation time, and time-sensitive connections.

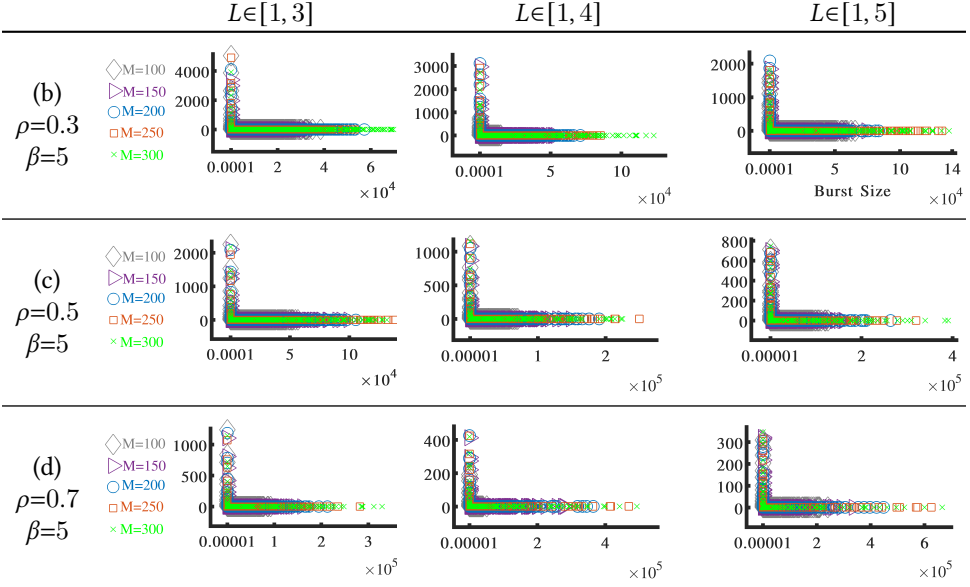


Table 9. Frequency (y axes) of burst sizes (x axes) in S-Amazon with 10^7 sgrs.

7 CONCLUSION

Butterflies are key building blocks of streaming bipartite graphs and their emergence patterns implies the growth patterns in streaming graphs. In this paper, we study the emergence of butterflies in streaming graphs displaying superlinear growth of butterfly count wrt the edge count. Integrating the connectivities, weights, and fine-grained temporal information, we investigate the strength assortativity of butterflies over the timeline of burst arrivals. We introduce a quantification approach for statistical analysis of confounding distributions that enable effective temporal analysis of strength assortativity in bipartite graphs with skewed strength distribution. Utilizing this approach, we unveil the "scale-invariant strength assortativity of streaming butterflies", a co-occurrence of three patterns: butterfly densification, strength diversification, and steady strength assortativity. We study the existing local rules for graph growth that yield skewed distributions, degree correlation, and cohesive structures to explain the observed mixing patterns. We find that implicit degree-driven preferential attachment and copying mechanisms or solely strength-driven preferential attachment with random assignment of timestamps to the edges can only partially preserve the observed patterns but are not effective enough to reproduce these patterns simultaneously. Therefore, we introduce a set of microscopic mechanisms, in the body of a proposed streaming growth model called *sGrow*, based on realistic streaming graph record generation, probabilistic connections, and strength-driven preferential random walks which explain the emergence patterns of streaming butterflies. *sGrow* is based on iterative addition of bursts of edges which satisfies streaming data model, preserves realistic patterns of butterfly emergence quantitatively and qualitatively, and makes the stream generation scalable. Moreover, *sGrow* enables generating sequence of bipartite edges attributed with timestamps and weights, isolated/out-of-order edges, and four-vertex graphlets. Our comprehensive evaluations validate the efficacy of *sGrow* in realization of streaming growth patterns effectively and independent of initial conditions, scale and temporal characteristics, and model configurations. Our analysis also verifies the robustness of *sGrow* in generating streaming graphs based on user-specified properties for the scale and burstiness of the stream, level of

strength assortativity, probability of-of-order streaming records, generation time, and time-sensitive connections. On top of the aforementioned advantages and qualified features, sGrow suits the following applications: (1) streaming graph benchmarks by generating configurable realistic data streams supported by a reference guide for parameter configuration and stress testing analysis, (2) machine learning benchmarks by providing annotated data streams which are synthesized by realistic instance injection and suit both testing and training purposes, and (3) development of streaming algorithms and models (e.g., concept drift models) by providing microscopic mechanisms and characteristic patterns that enlighten the architecture of model/algorithm.

REFERENCES

- [1] Rezwan Ahmed and George Karypis. Algorithms for mining the coevolving relational motifs in dynamic networks. *ACM Trans. Knowl. Discov. Data*, 10(1):1–31, 2015.
- [2] Leman Akoglu and Christos Faloutsos. Rtg: A recursive realistic graph generator using random typing. In *Joint European Conference on Machine Learning and Knowledge Discovery in Databases*, pages 13–28, 2009.
- [3] Leman Akoglu, Mary McGlohon, and Christos Faloutsos. Rtm: Laws and a recursive generator for weighted time-evolving graphs. In *Proc. 8th IEEE Int. Conf. on Data Mining*, pages 701–706, 2008.
- [4] Leman Akoglu, Mary McGlohon, and Christos Faloutsos. Oddball: Spotting anomalies in weighted graphs. In *Pacific-Asia Conf. on Knowledge Discovery and Data Mining*, pages 410–421, 2010.
- [5] Sinan G Aksoy, Cliff Joslyn, Carlos Ortiz Marrero, Brenda Praggastis, and Emilie Purvine. Hypernetwork science via high-order hypergraph walks. *EPJ Data Science*, 9(1):16, 2020.
- [6] Sinan G Aksoy, Tamara G Kolda, and Ali Pinar. Measuring and modeling bipartite graphs with community structure. *Journal of Complex Networks*, 5(4):581–603, 2017.
- [7] Marie Al-Ghossein, Talel Abdesslem, and Anthony BARRÉ. A survey on stream-based recommender systems. *ACM computing surveys (CSUR)*, 54(5):1–36, 2021.
- [8] Réka Albert and Albert-László Barabási. Statistical mechanics of complex networks. *Reviews of modern physics*, 74(1):47, 2002.
- [9] Barabasi Albert-Laszlo. The origin of bursts and heavy tails in human dynamics. *Nature*, 435(7039):207–211, 2005.
- [10] Sadegh Aliakbary, Jafar Habibi, and Ali Movaghar. Quantification and comparison of degree distributions in complex networks. In *7th Int. Symp. on Telecommunications*, pages 464–469, 2014.
- [11] Güneş Aluç, Olaf Hartig, M Tamer Özsu, and Khuzaima Daudjee. Diversified stress testing of rdf data management systems. In *Proc. 13th Int. Semantic Web Conf.*, pages 197–212, 2014.
- [12] Khaled Ammar and M Tamer Özsu. Wgb: Towards a universal graph benchmark. In *Advancing Big Data Benchmarks*, pages 58–72. 2013.
- [13] Naomi A Arnold, Raul J Mondragón, and Richard G Clegg. Likelihood-based approach to discriminate mixtures of network models that vary in time. *Scientific reports*, 11(1):1–13, 2021.
- [14] Albert-László Barabási and Réka Albert. Emergence of scaling in random networks. *Science*, 286(5439):509–512, 1999.
- [15] Michael J Barber. Modularity and community detection in bipartite networks. *Physical Review E*, 76(6):066102, 2007.
- [16] Alain Barrat, Marc Barthélemy, Romualdo Pastor-Satorras, and Alessandro Vespignani. The architecture of complex weighted networks. *Proc. National Academy of Sciences*, 101(11):3747–3752, 2004.
- [17] Alain Barrat, Marc Barthélemy, Romualdo Pastor-Satorras, and Alessandro Vespignani. Weighted evolving networks: coupling topology and weight dynamics. *Physical Review Letters*, 92(22):228701–228704, 2004.
- [18] Alain Barrat, Marc Barthélemy, and Alessandro Vespignani. Modeling the evolution of weighted networks. *Physical Review E*, 70(6):066149, 2004.
- [19] Austin R Benson, David F Gleich, and Jure Leskovec. Higher-order organization of complex networks. *Science*, 353(6295):163–166, 2016.
- [20] Ginestra Bianconi and A-L Barabási. Competition and multiscaling in evolving networks. In *The Structure and Dynamics of Networks*, pages 361–367. 2011.
- [21] Angela Bonifati, George Fletcher, Jan Hidders, and Alexandru Iosup. A survey of benchmarks for graph-processing systems. In *Graph Data Management*, pages 163–186. 2018.
- [22] Angela Bonifati, Irena Holubová, Arnau Prat-Pérez, and Sherif Sakr. Graph generators: State of the art and open challenges. *ACM computing surveys (CSUR)*, 53(2):1–30, 2020.
- [23] Guilherme O Campos, Arthur Zimek, Jörg Sander, Ricardo JGB Campello, Barbora Micenkova, Erich Schubert, Ira Assent, and Michael E Houle. On the evaluation of unsupervised outlier detection: measures, datasets, and an empirical study. *Data Mining and Knowledge Discovery*, 30(4):891–927, 2016.

- [24] Deepayan Chakrabarti and Christos Faloutsos. Graph mining: Laws, generators, and algorithms. *ACM computing surveys (CSUR)*, 38(1):2–es, 2006.
- [25] Lijun Chang, Jeffrey Xu Yu, Lu Qin, Hong Cheng, and Miao Qiao. The exact distance to destination in undirected world. *Vldb j.*, 21(6):869–888, 2012.
- [26] Vittoria Colizza, Alessandro Flammini, M Angeles Serrano, and Alessandro Vespignani. Detecting rich-club ordering in complex networks. *Nature physics*, 2(2):110–115, 2006.
- [27] Colin Cooper and Alan Frieze. A general model of web graphs. *Random Structures & Algorithms*, 22(3):311–335, 2003.
- [28] Peter Csermely, András London, Ling-Yun Wu, and Brian Uzzi. Structure and dynamics of core/periphery networks. *Journal of Complex Networks*, 1(2):93–123, 2013.
- [29] Gregorio D’Agostino, Antonio Scala, Vinko Zlatić, and Guido Caldarelli. Robustness and assortativity for diffusion-like processes in scale-free networks. *EPL (Europhysics Letters)*, 97(6):68006, 2012.
- [30] Manh Tuan Do, Se-eun Yoon, Bryan Hooi, and Kijung Shin. Structural patterns and generative models of real-world hypergraphs. In *Proc. 26th ACM SIGKDD Int. Conf. on Knowledge Discovery and Data Mining*, pages 176–186, 2020.
- [31] Zheng Dong, Xin Huang, Guorui Yuan, Hengshu Zhu, and Hui Xiong. Butterfly-core community search over labeled graphs. volume 14, pages 2006–2018, 2021.
- [32] Sergey N Dorogovtsev and José FF Mendes. Scaling properties of scale-free evolving networks: Continuous approach. *Physical Review E*, 63(5):056125, 2001.
- [33] Mikhail Drobyshvskiy and Denis Turdakov. Random graph modeling: A survey of the concepts. *ACM computing surveys (CSUR)*, 52(6):1–36, 2019.
- [34] Gideon Dror, Noam Koenigstein, Yehuda Koren, and Markus Weimer. The yahoo! music dataset and kdd-cup’11. In *Proc. KDD Cup 2011*, pages 3–18. PMLR, 2012.
- [35] Andrew F Emmott, Shubhomoy Das, Thomas Dietterich, Alan Fern, and Weng-Keen Wong. Systematic construction of anomaly detection benchmarks from real data. In *Proc. ACM SIGKDD workshop on outlier detection and description*, pages 16–21, 2013.
- [36] Yixiang Fang, Kai Wang, Xuemin Lin, and Wenjie Zhang. Cohesive subgraph search over big heterogeneous information networks: Applications, challenges, and solutions. In *Proc. ACM SIGMOD Int. Conf. on Management of Data*, pages 2829–2838, 2021.
- [37] Frank Fischer and Christoph Helmberg. Dynamic graph generation for the shortest path problem in time expanded networks. *Mathematical Programming*, 143(1):257–297, 2014.
- [38] Bailey K Fosdick, Daniel B Larremore, Joel Nishimura, and Johan Ugander. Configuring random graph models with fixed degree sequences. *Siam Review*, 60(2):315–355, 2018.
- [39] Dan Frankowski, Shyong K Lam, Shilad Sen, F Maxwell Harper, Scott Yilek, Michael Cassano, and John Riedl. Recommenders everywhere: the wikilens community-maintained recommender system. In *Proc. Int. Symposium on Wikis*, pages 47–60, 2007.
- [40] João Gama, André Zliobaitė, Albert Bifet, Mykola Pechenizkiy, and Abdelhamid Bouchachia. A survey on concept drift adaptation. *ACM computing surveys (CSUR)*, 46(4):1–37, 2014.
- [41] Michelle Girvan and Mark EJ Newman. Community structure in social and biological networks. *Proc. National Academy of Sciences*, 99(12):7821–7826, 2002.
- [42] Lukasz Golab and M Tamer Özsu. Data stream management. *Synthesis Lectures on Data Management*, 2(1):1–73, 2010.
- [43] Robert Görke, Roland Kluge, Andrea Schumm, Christian Staudt, and Dorothea Wagner. An efficient generator for clustered dynamic random networks. In *Mediterranean Conference on Algorithms*, pages 219–233, 2012.
- [44] Jelena Grujic, Marija Mitrovic, and Bosiljka Tadic. Mixing patterns and communities on bipartite graphs on web-based social interactions. In *16th Int. Conf. on Digital Signal Processing*, pages 1–8, 2009.
- [45] Xianbin Gu, Jeremiah D Deng, and Martin K Purvis. Superpixel-based segmentation using multi-layer bipartite graphs and grassmann manifolds. In *Proc. 29th Int. Conf. on Image and Vision Computing New Zealand*, pages 119–123, 2014.
- [46] Jean-Loup Guillaume and Matthieu Latapy. Bipartite structure of all complex networks. *Information processing letters*, 90(5):215–221, 2004.
- [47] Jean-Loup Guillaume and Matthieu Latapy. Bipartite graphs as models of complex networks. *Physica A: Statistical Mechanics and its Applications*, 371(2):795–813, 2006.
- [48] Roger Guimerà, Marta Sales-Pardo, and Luis A Nunes Amaral. Module identification in bipartite and directed networks. *Physical Review E*, 76(3):036102, 2007.
- [49] Guibing Guo, Jie Zhang, Daniel Thalmann, and Neil Yorke-Smith. Etaf: An extended trust antecedents framework for trust prediction. In *2014 IEEE/ACM Int. Conf. on Advances in Social Networks Analysis and Mining*, pages 540–547, 2014.
- [50] Ali Hadian, Sadegh Nobari, Behrooz Minaei-Bidgoli, and Qiang Qu. Roll: Fast in-memory generation of gigantic scale-free networks. In *Proc. ACM SIGMOD Int. Conf. on Management of Data*, pages 1829–1842, 2016.

- [51] Yang Hao, Mengqi Zhang, Xiaoyang Wang, and Chen Chen. Cohesive subgraph detection in large bipartite networks. In *32nd Int. Conf. on Scientific and Statistical Database Management*, pages 1–4, 2020.
- [52] F Maxwell Harper and Joseph A Konstan. The movielens datasets: History and context. *Acm transactions on interactive intelligent systems (tiis)*, 5(4):1–19, 2015.
- [53] Jonathan L Herlocker, Joseph A Konstan, Al Borchers, and John Riedl. An algorithmic framework for performing collaborative filtering. In *ACM SIGIR Forum*, volume 51, pages 227–234, 2017.
- [54] Petter Holme. Core-periphery organization of complex networks. *Physical Review E*, 72(4):046111, 2005.
- [55] Jiafeng Hu, Reynold Cheng, Kevin Chen-Chuan Chang, Aravind Sankar, Yixiang Fang, and Brian YH Lam. Discovering maximal motif cliques in large heterogeneous information networks. In *Proc. 35th Int. Conf. on Data Engineering*, pages 746–757. IEEE, 2019.
- [56] Jiewen Huang and Daniel J Abadi. Leopard: Lightweight edge-oriented partitioning and replication for dynamic graphs. *Proc. VLDB Endowment*, 9(7):540–551, 2016.
- [57] Shuta Ito and Takayasu Fushimi. Fast clustering of hypergraphs based on bipartite-edge restoration and node reachability. In *Proc. 22nd Int. Conf. on Information Integration and Web-based Applications & Services*, pages 115–124, 2020.
- [58] Mohsen Jamali, Gholamreza Haffari, and Martin Ester. Modeling the temporal dynamics of social rating networks using bidirectional effects of social relations and rating patterns. In *Proc. 20th Int. World Wide Web Conf.*, pages 527–536, 2011.
- [59] Jun Ji, Aifen Fang, Chenlu Qiu, and Lei Zhao. Detection of abnormal database queries in weighted bipartite graph. In *Proc. Int. Conf. on Big Data Engineering and Technology*, pages 7–11, 2018.
- [60] Ruoming Jin, Hui Hong, Haixun Wang, Ning Ruan, and Yang Xiang. Computing label-constraint reachability in graph databases. In *Proc. ACM SIGMOD Int. Conf. on Management of Data*, pages 123–134, 2010.
- [61] Nitin Jindal and Bing Liu. Opinion spam and analysis. In *Proc. Int. Conf. Web Search and Web Data Mining*, pages 219–230, 2008.
- [62] Jon M Kleinberg, Ravi Kumar, Prabhakar Raghavan, Sridhar Rajagopalan, and Andrew S Tomkins. The web as a graph: Measurements, models, and methods. In *Int. Computing and Combinatorics Conf.*, pages 1–17, 1999.
- [63] Lauri Kovanen, Márton Karsai, Kimmo Kaski, János Kertész, and Jari Saramäki. Temporal motifs in time-dependent networks. *Journal of Statistical Mechanics: Theory and Experiment*, 2011(11):P11005, 2011.
- [64] Pavel L Krapivsky and Sidney Redner. Network growth by copying. *Physical Review E*, 71(3):036118, 2005.
- [65] Pavel L Krapivsky, Geoff J Rodgers, and Sidney Redner. Degree distributions of growing networks. *Physical Review Letters*, 86(23):5401, 2001.
- [66] Ravi Kumar, Prabhakar Raghavan, Sridhar Rajagopalan, D Sivakumar, Andrew Tomkins, and Eli Upfal. Stochastic models for the web graph. In *Proceedings 41st Annual Symposium on Foundations of Computer Science*, pages 57–65, 2000.
- [67] Jérôme Kunegis. Konect: the koblenz network collection. In *Proc. 22nd Int. World Wide Web Conf.*, pages 1343–1350, 2013.
- [68] Matthieu Latapy, Clémence Magnien, and Nathalie Del Vecchio. Basic notions for the analysis of large two-mode networks. *Social Networks*, 30(1):31–48, 2008.
- [69] Jure Leskovec, Lars Backstrom, Ravi Kumar, and Andrew Tomkins. Microscopic evolution of social networks. In *Proc. 14th ACM SIGKDD Int. Conf. on Knowledge Discovery and Data Mining*, pages 462–470, 2008.
- [70] Jure Leskovec, Jon Kleinberg, and Christos Faloutsos. Graphs over time: densification laws, shrinking diameters and possible explanations. In *Proc. 11th ACM SIGKDD Int. Conf. on Knowledge Discovery and Data Mining*, pages 177–187, 2005.
- [71] Jure Leskovec, Jon Kleinberg, and Christos Faloutsos. Graph evolution: Densification and shrinking diameters. *ACM Trans. Knowl. Discov. Data*, 1(1):2–es, 2007.
- [72] CC Leung and HF Chau. Weighted assortative and disassortative networks model. *Physica A: Statistical Mechanics and its Applications*, 378(2):591–602, 2007.
- [73] Rundong Li, Pinghui Wang, Peng Jia, Xiangliang Zhang, Junzhou Zhao, Jing Tao, Ye Yuan, and Xiaohong Guan. Approximately counting butterflies in large bipartite graph streams. *IEEE Trans. Knowl. and Data Eng.*, 2021.
- [74] Xiaodong Li, Reynold Cheng, Kevin Chen-Chuan Chang, Caihua Shan, Chenhao Ma, and Hongtai Cao. On analyzing graphs with motif-paths. volume 14, pages 1111–1123, 2021.
- [75] Ee-Peng Lim, Viet-An Nguyen, Nitin Jindal, Bing Liu, and Hady Wirawan Lauw. Detecting product review spammers using rating behaviors. In *Proc. 19th ACM Int. Conf. on Information and Knowledge Management*, pages 939–948, 2010.
- [76] Kun Liu and Evimaria Terzi. Towards identity anonymization on graphs. In *Proc. ACM SIGMOD Int. Conf. on Management of Data*, pages 93–106, 2008.
- [77] Paul Liu, Austin R Benson, and Moses Charikar. Sampling methods for counting temporal motifs. In *Proc. 12th ACM Int. Conf. Web Search and Data Mining*, pages 294–302, 2019.

- [78] Weide Liu, Chi Zhang, Guosheng Lin, Tzu-Yi Hung, and Chunyan Miao. Weakly supervised segmentation with maximum bipartite graph matching. In *Proc. 28th ACM Int. Conf. on Multimedia*, pages 2085–2094, 2020.
- [79] Chenhao Ma, Reynold Cheng, Laks VS Lakshmanan, Tobias Grubenmann, Yixiang Fang, and Xiaodong Li. Linc: a motif counting algorithm for uncertain graphs. *Proc. VLDB Endowment*, 13(2):155–168, 2019.
- [80] Mary McGlohon, Leman Akoglu, and Christos Faloutsos. Weighted graphs and disconnected components: patterns and a generator. In *Proc. 14th ACM SIGKDD Int. Conf. on Knowledge Discovery and Data Mining*, pages 524–532, 2008.
- [81] Ron Milo, Shai Shen-Orr, Shalev Itzkovitz, Nadav Kashtan, Dmitri Chklovskii, and Uri Alon. Network motifs: simple building blocks of complex networks. *Science*, 298(5594):824–827, 2002.
- [82] Jayanta Mondal and Amol Deshpande. Managing large dynamic graphs efficiently. In *Proc. ACM SIGMOD Int. Conf. on Management of Data*, pages 145–156, 2012.
- [83] Arjun Mukherjee, Bing Liu, and Natalie Glance. Spotting fake reviewer groups in consumer reviews. In *Proc. 21st Int. World Wide Web Conf.*, pages 191–200, 2012.
- [84] Mark EJ Newman. Assortative mixing in networks. *Physical Review Letters*, 89(20):208701, 2002.
- [85] Mark EJ Newman and Juyong Park. Why social networks are different from other types of networks. *Physical Review E*, 68(3):036122, 2003.
- [86] Mark EJ Newman, Steven H Strogatz, and Duncan J Watts. Random graphs with arbitrary degree distributions and their applications. *Physical Review E*, 64(2):026118, 2001.
- [87] Rogier Noldus and Piet Van Mieghem. Assortativity in complex networks. *Journal of Complex Networks*, 3(4):507–542, 2015.
- [88] M Tamer Özsu and Valduriez Patrick. Big data processing. *Principles of Distributed Database Systems*, pages 449–518, 2019.
- [89] M Tamer Özsu and Valduriez Patrick. Stream data management. *Principles of Distributed Database Systems*, pages 470–485, 2019.
- [90] Ashwin Paranjape, Austin R Benson, and Jure Leskovec. Motifs in temporal networks. In *Proc. 10th ACM Int. Conf. Web Search and Data Mining*, pages 601–610, 2017.
- [91] Deokhwan Park, Joosoon Lee, Junseok Lee, and Kyoobin Lee. Deep learning based food instance segmentation using synthetic data. In *2021 18th Int. Conf. on Ubiquitous Robots (UR)*, pages 499–505, 2021.
- [92] Himchan Park and Min-Soo Kim. Lineageba: A fast, exact and scalable graph generation for the barabási-albert model. In *Proc. 37th Int. Conf. on Data Engineering*, pages 540–551, 2021.
- [93] Romualdo Pastor-Satorras, Alexei Vázquez, and Alessandro Vespignani. Dynamical and correlation properties of the internet. *Physical Review Letters*, 87(25):258701, 2001.
- [94] Tiago P. Peixoto. The netzschleuder network catalogue and repository, 2020.
- [95] Sumit Purohit, Lawrence B Holder, and George Chin. Temporal graph generation based on a distribution of temporal motifs. In *Proceedings of the 14th International Workshop on Mining and Learning with Graphs*, volume 7, 2018.
- [96] Jérémie Rappaz, Julian McAuley, and Karl Aberer. Recommendation on live-streaming platforms: Dynamic availability and repeat consumption. *Interactions*, 20:40, 2021.
- [97] Ryan A Rossi, Nesreen K Ahmed, Aldo Carranza, David Arbour, Anup Rao, Sungchul Kim, and Eunye Koh. Heterogeneous graphlets. *ACM Trans. Knowl. Discov. Data*, 15(1):1–43, 2020.
- [98] Aida Sheshbolouki and M Tamer Özsu. sgrapp: Butterfly approximation in streaming graphs. *ACM Trans. Knowl. Discov. Data (Accepted for publication)*, 2021. Available at: <https://arxiv.org/abs/2101.12334>.
- [99] Aida Sheshbolouki, Mina Zarei, and Hamid Sarbazi-Azad. Are feedback loops destructive to synchronization? *EPL (Europhysics Letters)*, 111(4):40010, 2015.
- [100] Yook Soon-Hyung, Hawoong Jeong, Albert-Laszlo Barabási, and Yuhai Tu. Weighted evolving networks. *Physical Review Letters*, 86:5835–5838, 2001.
- [101] Isabelle Stanton and Ali Pinar. Constructing and sampling graphs with a prescribed joint degree distribution. *Journal of Experimental Algorithmics (JEA)*, 17:3–1, 2012.
- [102] Jianing Sun, Yingxue Zhang, Wei Guo, Huifeng Guo, Ruiming Tang, Xiuqiang He, Chen Ma, and Mark Coates. Neighbor interaction aware graph convolution networks for recommendation. In *Proc. 43rd Annual Int. ACM SIGIR Conf. on Research and Development in Information Retrieval*, page 1289–1298, 2020.
- [103] Zeeshan Syed, Collin Stultz, Manolis Kellis, Piotr Indyk, and John Guttat. Motif discovery in physiological datasets: a methodology for inferring predictive elements. *ACM Trans. Knowl. Discov. Data*, 4(1):1–23, 2010.
- [104] Jiliang Tang, Huiji Gao, Huan Liu, and Atish Das Sarma. etrust: Understanding trust evolution in an online world. In *Proc. 18th ACM SIGKDD Int. Conf. on Knowledge Discovery and Data Mining*, pages 253–261, 2012.
- [105] Yu Ting, Cao Yan, and Mu Xiang-wei. Personalized recommendation system based on web log mining and weighted bipartite graph. In *2013 Int. Conf. on Computational and Information Sciences*, pages 587–590, 2013.
- [106] Stojan Trajanovski, Javier Martín-Hernández, Wynand Winterbach, and Piet Van Mieghem. Robustness envelopes of networks. *Journal of Complex Networks*, 1(1):44–62, 2013.

- [107] Katherine Van Koeveering, Austin R Benson, and Jon Kleinberg. Random graphs with prescribed k -core sequences: A new null model for network analysis. *arXiv preprint arXiv:2102.12604*, 2021.
- [108] Demival Vasques Filho and Dion RJ O’Neale. Degree distributions of bipartite networks and their projections. *Physical Review E*, 98(2):022307, 2018.
- [109] Demival Vasques Filho and Dion RJ O’Neale. Transitivity and degree assortativity explained: The bipartite structure of social networks. *Physical Review E*, 101(5):052305, 2020.
- [110] Alexei Vazquez. Knowing a network by walking on it: emergence of scaling. *arXiv preprint cond-mat/0006132*, 2000.
- [111] Alexei Vázquez. Growing network with local rules: Preferential attachment, clustering hierarchy, and degree correlations. *Physical Review E*, 67(5):056104, 2003.
- [112] Andrew Z. Wang, Rex Ying, Pan Li, Nikhil Rao, Karthik Subbian, and Jure Leskovec. Bipartite dynamic representations for abuse detection. In *Proc. 26th ACM SIGKDD Int. Conf. on Knowledge Discovery and Data Mining*, page 3638–3648, 2021.
- [113] Kai Wang, Xuemin Lin, Lu Qin, Wenjie Zhang, and Ying Zhang. Vertex priority based butterfly counting for large-scale bipartite networks. *Proc. VLDB Endowment*, 12(10):1139–1152, 2019.
- [114] Wei Wang, Furu Wei, Wenjie Li, and Sujian Li. Hypersum: hypergraph based semi-supervised sentence ranking for query-oriented summarization. In *Proc. 18th ACM Int. Conf. on Information and Knowledge Management*, pages 1855–1858, 2009.
- [115] Duncan J Watts and Steven H Strogatz. Collective dynamics of ‘small-world’ networks. *Nature*, 393(6684):440, 1998.
- [116] Anatol Wegner. Random graphs with motifs. 2011.
- [117] Yinwei Wei, Xiang Wang, Liqiang Nie, Xiangnan He, Richang Hong, and Tat-Seng Chua. Mmgcn: Multi-modal graph convolution network for personalized recommendation of micro-video. In *Proc. 27th ACM Int. Conf. Multimedia*, pages 1437–1445, 2019.
- [118] Guangyu Wu, Martin Harrigan, and Pádraig Cunningham. Characterizing wikipedia pages using edit network motif profiles. In *Proc. 3rd int. workshop on Search and mining user-generated contents*, pages 45–52, 2011.
- [119] Shengqi Yang, Xifeng Yan, Bo Zong, and Arijit Khan. Towards effective partition management for large graphs. In *Proc. ACM SIGMOD Int. Conf. on Management of Data*, pages 517–528, 2012.
- [120] Josh Jia-Ching Ying, Ji Zhang, Che-Wei Huang, Kuan-Ta Chen, and Vincent S Tseng. Fraudetector+ an incremental graph-mining approach for efficient fraudulent phone call detection. *ACM Trans. Knowl. Discov. Data*, 12(6):1–35, 2018.
- [121] Giselle Zeno, Timothy La Fond, and Jennifer Neville. Dymond: Dynamic motif-nodes network generative model. In *Proceedings of the Web Conference 2021*, pages 718–729, 2021.
- [122] Yang Zhang. Language in our time: An empirical analysis of hashtags. In *Proc. 28th Int. World Wide Web Conf.*, pages 2378–2389, 2019.
- [123] Lingxiao Zhao and Leman Akoglu. On using classification datasets to evaluate graph outlier detection: Peculiar observations and new insights. *arXiv preprint arXiv:2012.12931*, 2020.
- [124] Yi Zheng, Hongchao Qin, Jun Zheng, Fusheng Jin, and Rong-Hua Li. Butterfly-based higher-order clustering on bipartite networks. In *Int. Conf. on Knowledge Science, Engineering and Management*, pages 485–497, 2020.
- [125] Zheng Zhong, Shen Yan, Zikun Li, Decheng Tan, Tong Yang, and Bin Cui. Bursts sketch: Finding bursts in data streams. In *Proc. ACM SIGMOD Int. Conf. on Management of Data*, pages 2375–2383, 2021.
- [126] Dawei Zhou, Lecheng Zheng, Jiawei Han, and Jingrui He. A data-driven graph generative model for temporal interaction networks. In *Proc. 26th ACM SIGKDD Int. Conf. on Knowledge Discovery and Data Mining*, pages 401–411, 2020.
- [127] Shi Zhou and Raúl J Mondragón. The rich-club phenomenon in the internet topology. *IEEE communications letters*, 8(3):180–182, 2004.
- [128] Tao Zhou, Jie Ren, Matúš Medo, and Yi-Cheng Zhang. Bipartite network projection and personal recommendation. *Physical Review E*.
- [129] Qiuyu Zhu, Jiahong Zheng, Hao Yang, Chen Chen, Xiaoyang Wang, and Ying Zhang. Hurricane in bipartite graphs: The lethal nodes of butterflies. In *32nd Int. Conf. on Scientific and Statistical Database Management*, pages 1–4, 2020.
- [130] Yong Zou, Reik V Donner, Norbert Marwan, Jonathan F Donges, and Jürgen Kurths. Complex network approaches to nonlinear time series analysis. *Physics Reports*, 787:1–97, 2019.